Adjacent versus Opposite Type Di-Aromatic Ring-Fused Phthalocyanine Derivatives: Synthesis, Spectroscopy, Electrochemistry, and Molecular Orbital Calculations

3 AUTHORS, INCLUDING:

Nagao Kobayashi
Tohoku University

529 PUBLICATIONS   **11,326** CITATIONS

SEE PROFILE

Victor N Nemykin
University of Minnesota Duluth

202 PUBLICATIONS   **2,589** CITATIONS

SEE PROFILE

Adjacent versus *Opposite* Type Di-Aromatic Ring-Fused Phthalocyanine Derivatives: Synthesis, Spectroscopy, Electrochemistry, and Molecular Orbital Calculations

Nagao Kobayashi,* Hideya Miwa, and Victor N. Nemykin

Contribution from the Department of Chemistry, Graduate School of Science, Tohoku University, Sendai 980-8578, Japan

Abstract: A series of adjacent and opposite type di-aromatic ring-fused phthalocyanines (Pc's) of varying size have been prepared and characterized spectroscopically and electrochemically, and most of their properties have been reasonably reproduced by molecular orbital (MO) calculations. The adjacent isomers alone were obtained preferentially by using a diphthalonitrile unit linked via a short aryl chain. The main results are summarized as follows. (i) The Q-band shifts to longer wavelength and its intensity increases, but the degree of change decreases, with increasing molecular size. On the bases of the experiments and MO calculations, setting the size of the effect of benzene directly fused to the tetraazaporphyrin (TAP) skeleton at unity, the effect of the second and third benzene units is roughly about 0.75−0.80 and 0.48 ± 0.06, respectively. As a result of this, among compounds having an isomeric π-system, the Q-band of a D_{4h} type species lies at longer wavelength than those of adjacently and oppositely di-aromatic ring-fused species. (ii) The Q-band of adjacently substituted species does not split appreciably, while that of the oppositely substituted species splits substantially, the extent having a parallel relationship with the ratio of long to short axes in the molecule. In general, the larger the ratio, the larger the splitting. (iii) The Q-band of oppositely dibenzo-fused and bis(dialkyl)-substituted TAP does not show explicit splitting because of the large coefficients of the carbons substituted with alkyl groups in the MOs. (iv) Interestingly, the first oxidation in adjacently and oppositely dibenzo-fused CoTAP occurs at the cobalt and ligand, respectively, although they are isomers to each other.

Introduction

In the past decade, research on low symmetrical phthalocyanines (Pc's) has been popular among Pc chemists.[1−3] Low symmetrical Pc's are more suitable for several purposes than low symmetrical porphyrins. For example, the Q-band transition in the visible region has much more allowed character than that in porphyrins;[4] therefore, adjustment of the color is easier. In addition, the correspondence between experiments and quantum chemical calculations is also generally better, since the HOMO−LUMO transition is essentially explained by a one-electron description.[5] Monosubstituted type low symmetrical Pc derivatives have been prepared either by mixed condensation reaction,[6,7] polymer support method,[8] or ring-expansion reaction of subphthalocyanines.[9] Disubstituted analogues have so far been obtained only by mixed condensation of two kinds of aromatic ortho dinitriles or isoindolediimines, which gave mixtures of products, and subsequent tedious purification by column

(1) *Phthalocyanines−Properties and Applications*; Leznoff, C. C., Lever, A. B. P., Eds.; VCH Publishers: New York, 1989 (Vol. 1), 1992 (Vol. 2), 1993 (Vol. 3), and 1996 (Vol. 4).

(2) Kobayashi, N. In ref 1, Vol. 1, Chapter 3.

(3) Some representative ones: (a) Kobayashi, N.; Ashida, T.; Osa, T. *Chem. Lett.* **1992**, 1567, 2031. (b) Konami, H.; Ikeda, Y.; Hatano, M.; Mochiziki, K. *Mol. Phys.* **1993**, *80*, 153. (c) Kobayashi, N.; Ashida, T.; Osa, T.; Konami, H. *Inorg. Chem.* **1994**, *33*, 1735. (d) Baumann, T. F.; Sibert, J. W.; Olmstead, M. M.; Barrett, A. G. M.; Hoffman, B. M. *J. Am. Chem. Soc.* **1994**, *116*, 2639. (e) Nemykin, V. N.; Subbotin, N. B.; Kostromina, N. A.; Volkov, S. V.; Luk'yanets, E. A. *Russ. J. Inorg. Chem.* **1995**, *40*, 1141. (f) Kobayashi, N.; Togashi, M.; Osa, T.; Ishii, K.; Yamauchi, S.; Hino, H. *J. Am. Chem. Soc.* **1996**, *118*, 1073. (g) Baumann, T. F.; Nasier, M. S.; Sibert, J. W.; White, A. J. P.; Olmstead, M. M.; Williams, D. J.; Barrett, A. G. M.; Hoffman, B. M. *J. Am. Chem. Soc.* **1996**, *118*, 10479. (h) Humberstone, P.; Clarkson, G. J.; McKeown, N. B.; Treacher, K. E. *J. Mater. Chem.* **1996**, *6*, 315. (i) Leznoff, C. C.; Drew, D. M. *Can. J. Chem.* **1996**, *74*, 307. (j) Nolan, K. J. M.; Hu, M.; Leznoff, C. C. *Synlett* **1997**, 593. (k) Cook, M. J.; Jafari-Fini, A. *J. Mater. Chem.* **1997**, *7*, 5. (l) Dabak, S.; Bekaroglu, O. *J. Chem. Res.* **1997**, 8. (m) Aoudia, M.; Cheng, G.; Kennedy, V. O.; Kenney, M. E.; Rodgers, M. A. J. *J. Am. Chem. Soc.* **1997**, *119*, 6029. (n) Rodriguez-Morgade, S.; Hanack, M. *Chem. Eur. J.* **1997**, *3*, 1042. (o) Forsyth, T. P.; Williams, D. B. G.; Montalban, A. G.; Stern, C. L.; Barrett, A. G. M.; Hoffman, B. M. *J. Org. Chem.* **1998**, *63*, 331. (p) Maya, E. M.; Vazquez, P.; Torres, T. *Chem. Eur. J.* **1999**, *7*, 2004. (q) Kobayashi, N.; Miwa, H.; Isago, H.; Tomura, T. *Inorg. Chem.* **1999**, *38*, 479. (r) Miwa, H.; Kobayashi, N. *Chem. Lett.* **1999**, 1303. (s) Cabezon, B. C.; Nicolau, M.; Barbera, J.; Torres, T. *Chem. Mater.* **2000**, *12*, 776. (t) Cabezon, B.; Quesada, E.; Esperanza, S.; Torres, T. *Eur. J. Org. Chem.* **2000**, 2767. (u) De la Torre, G.; Claessens, C. G.; Torres, T. *Eur. J. Org. Chem.* **2000**, 2821.

(4) Gouterman, M. In *The Porphyrins*; Dolphin, D., Ed.; Academic Press: New York, 1978; Vol. 3, Chapter 1.

(5) Kobayashi, N.; Konami, H. In ref 1, Vol. 4, Chapter 9.

(6) Leznoff, C. C. In ref 1, Vol. 1, Chapter 1.

(7) Piechocki, C.; Simon, J. *J. Chem. Soc., Chem. Commun.* **1985**, 259.

(8) (a) Leznoff, C. C.; Hall, T. W. *Tetrahedron Lett.* **1982**, *23*, 3023. (b) Hall, T. W.; Greenberg, S.; McArthur, C. R.; Khouw, B.; Leznoff, C. C. *Nouv. J. Chim.* **1982**, *6*, 653. (c) Wohrle, D.; Krawczyk, G. *Polym. Bull.* **1986**, *15*, 193. (d) Leznoff, C. C.; Svirskaya, P. I.; Khouw, B.; Cerny, R. L.; Seymour, P.; Lever, A. B. P. *J. Org. Chem.* **1991**, *56*, 82.

(9) (a) Kobayashi, N.; Kondo, R.; Nakajima, S.; Osa, T. *J. Am. Chem. Soc.* **1990**, *112*, 9640. (b) Kobayashi, N.; Ishizaki, T.; Ishii, K.; Konami, H. *J. Am. Chem. Soc.* **1999**, *121*, 9096. (c) Kobayashi, N. *J. Porphyrins Phthalocyanines* **1999**, *3*, 453. (d) Sastre, A.; Del Rey, B.; Torres, T. *J. Org. Chem.* **1996**, *61*, 8591.

chromatography.[3a,c,e,g,m,n] However, the separation and identification of adjacently (C_{2v} type) and oppositely substituted (D_{2h} type) Pc's are generally particularly difficult, since their molecular weights are identical. To date, adjacent and opposite dibenzo-substituted Pc's have been prepared and compared,[3b,m,n] but no one has prepared and characterized a series of adjacently and oppositely substituted Pc's of varying size. In the work described in this paper, we have prepared these types of cobalt Pc derivative and compared their spectroscopic and electrochemical properties (Figure 1). Some of the experimental results are interpreted using the results of molecular orbital (MO) calculations. As will be shown below, adjacently and oppositely di-aromatic ring-fused Pc analogues have indeed strikingly contrasting spectroscopic properties. In a few cases, the experimentally obtained characteristics were different from those expected theoretically. However, reasonable interpretations have been eventually given.

Because of the solubility problem and the academic interest, a series of cobalt complexes were prepared. Zinc and nickel complexes are desirable from the standpoint of structural analysis, since NMR spectroscopy is available. However, naphthalene- and anthracene-fused zinc complexes decomposed during column chromatography, while the low yield and low solubility of anthracene-fused nickel complex prevented us from preparing a series of nickel complexes. Cobalt complexes alone had solubility and stability enough for characterization. Accordingly, cobalt was chosen as a central metal atom.

Experimental Section

(i) Measurements. The 400 MHz ^{1}H NMR spectral measurements were made with a JEOL GSX-400 instrument. Mass spectra were measured with a Perspective Biosystem MALDI-TOF Mass Voyager DE-SI2 spectrometer using dithranol (1,8,9-anthracenetriol) as a matrix, with a JEOL JMS-HX110 mass spectrometer (FAB mass) using *m*-nitrobenzyl alcohol (NBA) as a matrix and with a Micromass LCT (ESI-TOF mass) using chloroform and methanol as solvents. Electronic absorption spectra were measured with a Hitachi U-3410 spectrophotometer. Magnetic circular dichroism (MCD) spectra were run on a Jasco J-725 spectrodichrometer using toluene (Nacalai Tesque, for adjacent species) or *o*-dichlorobenzene (*o*-DCB) (Nacalai Tesque, HPLC grade, for opposite species) solutions of ca. $10^{-5}-10^{-6}$ mol/L because of the solubility problem and in an attempt to obtain nonaggregated spectra, with a Jasco electromagnet that produces magnetic fields of up to 1.09 T. The magnitude was expressed in terms of molar ellipticity per tesla, $[\theta]_M/10^4$ deg mol^{-1} cm^{-3} cm^{-1} T^{-1}.

Cyclic voltammetry data were collected with a Hokuto Denko HA-501 potentiostat connected to a Graphtec WX1200 *XY* recorder. Differential pulse voltammetry data were recorded with a Yanaco P-1100 polarographic analyzer connected to a Watanabe WX 4401 *XY* recorder. Electrochemical experiments were performed under purified nitrogen gas. A glassy carbon working electrode (area = 0.07 cm^2) and a Pt wire counter electrode were employed. The reference electrode was Ag/AgCl, corrected for junction potentials by referencing internally to the Fc$^+$/Fc couple. In the solution used, i.e., in *o*-DCB (Nacalai Tesque, HPLC grade) containing 0.1 mol/L tetrabutylammonium perchlorate (TBAP), the Fc$^+$/Fc couple was observed at approximately 0.51 ± 0.02 V vs Ag/AgCl. For spectroelectrochemical measurements, an optically transparent thin-layer electrode (OTTLE) cell of path length 1 mm was employed using a Pt minigrid as both the working and counter electrodes, respectively,[10] and a TBAP concentration of 0.3 mol/L.

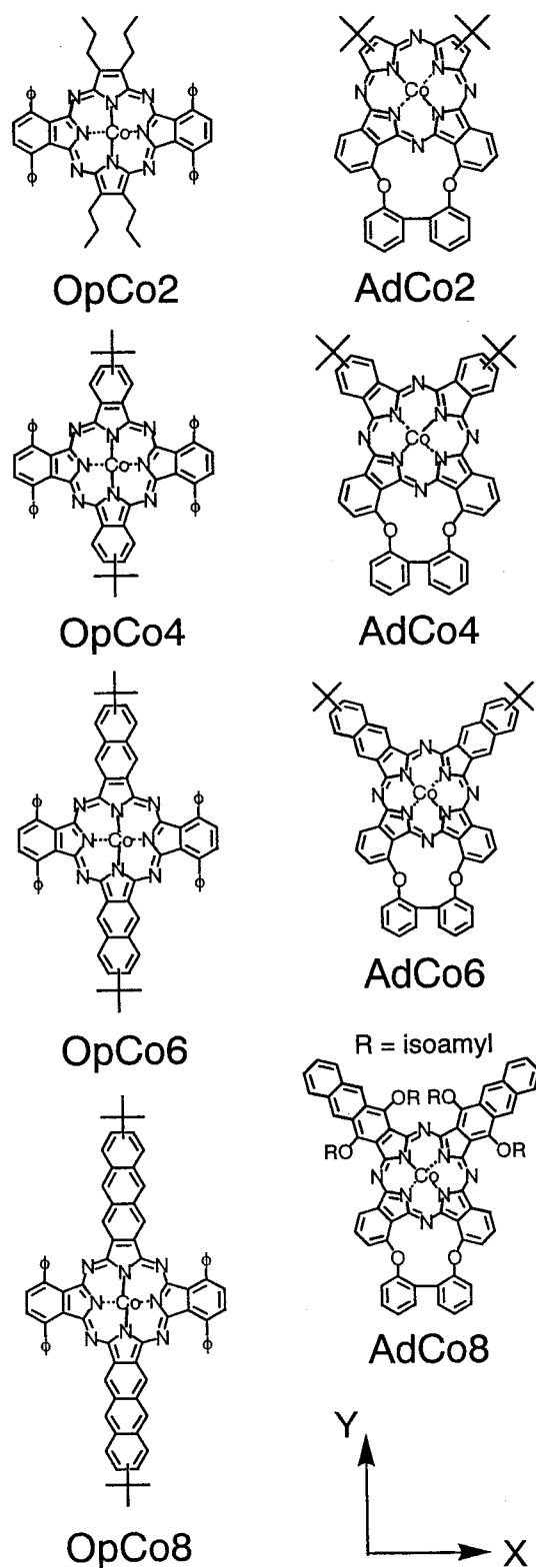(10) Kobayashi, N.; Nishiyama, Y. *J. Phys. Chem.* **1985**, *89*, 1167.

Figure 1. Structures and abbreviations of the compounds in this study, and the directions of *x*- and *y*-axes in each compound. "Ad" and "Op" mean "adjacent" and "opposite", respectively, and the numbers at the end indicate the number of benzene units fused to the tetraazaporphyrin (TAP) skeleton.

Crystal structural analysis of an oppositely substituted compound was performed on a Rigaku/MSC Mercury diffractometer with graphite-monochromated Mo Kα radiation (λ = 0.7107 Å). All calculations were performed using the teXsan crystallographic software package[11] on a Silicon Graphics O$_2$ computer.

Scheme 1. Synthesis of Adjacent Type Species
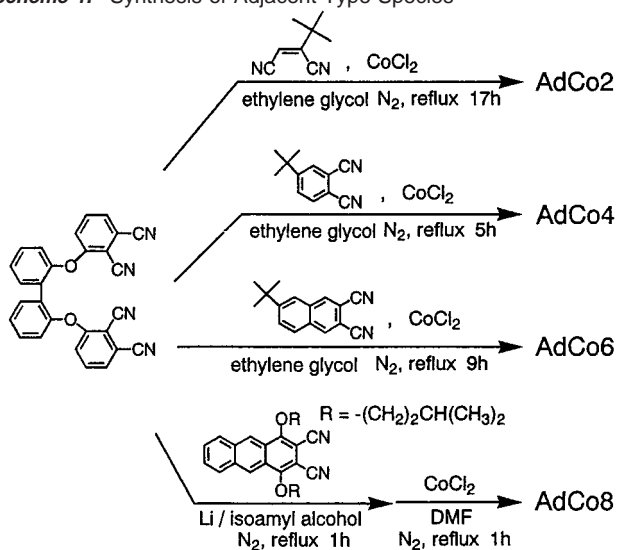
(ii) Molecular Orbital Calculations. MO calculations were performed by the ZINDO/S Hamiltonian in the HyperChem R.5.1 program[12a] which has been successfully applied to Pc systems.[12b,c] The structures of Pc analogues for calculations were constructed by using X-ray structural data of standard Pc,[13] naphthalene,[14a] and anthracene[14b] and by making the rings perfectly planar and adopting either the C_{2v} or D_{2h} symmetry (essentially the same as those we used in our previous papers).[5,15] The central metal was assumed to be zinc(II) since Co(II) is paramagnetic. However, to interpret the spectra of low symmetrical closed-shell d^8 Co(I) species, calculations were similarly performed for two π systems. The choice of configuration was based on energetic considerations, and all singly excited configurations up to 9 eV (72 590 cm^{-1}) were included.

(iii) Synthesis. Adjacently substituted compounds were prepared according to the pathway shown in Scheme 1. To prevent the formation of opposite type species, a diphthalonitrile unit linked by the ortho positions of biphenyl, i.e., 2,2′-bis(2,3-dicyanophenoxy)biphenyl,[3q] was used. Opposite type compounds were obtained by normal mixed condensation reactions utilizing the steric hindrance of one of the starting dinitriles, i.e., 3,6-diphenylphthalonitrile.[3a,16] OpCo2, OpCo4, and OpCo6 were obtained by cobalt insertion reaction into the corresponding metal-free species whose D_{2h} π structures were predetermined by ^{1}H NMR and electronic absorption spectra. The tetra-*tert*-butylated tetraazaporphyrin cobalt complex (Co0) was that which we used in our earlier papers.[17] *tert*-Butylated dinitriles,[17b,18-20] 2,3-dicyano-1,4-diisoamylanthracene,[3r] and dipropylfumalonitrile[21] were prepared

(11) *teXan: Crystal Structure Analysis Package*; Molecular Structure Corp., The Woodlands, TX, 1985 and 1999.
(12) (a) *HyperChem R.5.1 Pro*; Hypercube Inc., Gainesville, FL, 1997. (b) Mack, J.; Stillman, M. J. *Inorg. Chem.* **1997**, *36*, 413. (c) Cory, M. G.; Hirose, H.; Zerner, M. C. *Inorg. Chem.* **1995**, *34*, 2969.
(13) Robertson, J. M.; Woodward, I. *J. Chem. Soc.* **1937**, 219. Barrett, P. A.; Dent, C. E.; Linstead, R. P. *J. Chem. Soc.* **1936**, 1719. Brown, C. J. *J. Chem. Soc. A* **1968**, 2488; 2494. Kirner, J. F.; Dow, W.; Scheidt, D. R. *Inorg. Chem.* **1976**, *15*, 1685.
(14) (a) House, H. O.; Koepsell, D. G.; Campbell, W. J. *J. Org. Chem.* **1972**, *37*, 1003. (b) Fillers, J. P.; Ravichsandran, K. G.; Abdalmuhdi, I.; Chang, C. K. *J. Am. Chem. Soc.* **1986**, *108*, 417.
(15) Kobayashi, N.; Konami, H. *J. Porphyrins Phthalocyanines* **2001**, *5*, 233.
(16) Mikhalenko, S. A.; Gladyr, S. A.; Luk'yanets, E. A. *J. Org. Chem. USSR* **1972**, *8*, 341.
(17) (a) Kobayashi, N.; Nakajima, S.; Osa, T. *Chem. Lett.* **1992**, 2415. (b) Kobayashi, N.; Nakajima, S.; Osa, T. *Inorg. Chim. Acta* **1993**, *210*, 131.
(18) Kopranenkov, V. N.; Goncharova, L. S.; Luk'yanets, E. A. *J. Gen. Chem. USSR* **1977**, *47*, 1954.
(19) Kovshev, E. I.; Punchanova, V. A.; Luk'yanets, E. A. *J. Gen. Chem. USSR* **1971**, *7*, 364.
(20) *Phthalocyanines—Chemistry and Functions*; Shirai, H., Kobayashi, N., Eds.; IPC Publishers: Tokyo, 1997 (in Japanese).
(21) Lange, S. J.; Nie, H.; Stern, C. L.; Barrett, A. G. M.; Hoffman, B. M. *Inorg. Chem.* **1998**, *37*, 6435.

as previously reported. 4-*tert*-Butylphthalonitrile (Tokyo Kasei) was used as supplied. Isotropic distribution patterns of the mass spectra of the following compounds are given in the Supporting Information.

[2^4,7^1-(2,2′-Biphenyldioxy)dibenzo[*b,g*]-12(or 13),17(or 18)-di-*tert*-butyl-5,10,15,20-tetraazaporphyrinato(2−)]cobalt(II), AdCo2. A mixture of 2,2′-bis(2,3-dicyanophenoxy)biphenyl[3q] (367 mg, 8.37 × 10^{-4} mol), *cis*-1,2-dicyano-3,3-dimethyl-1-butene[18] (218 mg, 1.62 × 10^{-3} mol), dried cobalt dichloride (106 mg, 8.16 × 10^{-4} mol), and a catalytic amount of ammonium molybdate was refluxed in ethylene glycol (4 mL) for 17 h under nitrogen, and after cooling the residue was collected by filtration, washed with water, and dried. The residue was imposed on silica gel chromatography using hexane/toluene (1:1 v/v) as eluent. The fourth colored fraction, which eluted after the first purplish red, second blue, and third purplish red fractions, was collected and further chromatographed over silica gel using hexane/chloroform (2:3 v/v) as eluent. Addition of methanol and water caused precipitation (11 mg, 1.8%) of a dark blue powder of the desired compound. Mass (FAB) (*m/z*): 766 (M$^+$). Anal. Found: C, 67.41; H, 4.84; N, 14.35. Calcd for C$_{44}$H$_{34}$N$_8$O$_2$Co·H$_2$O: C, 67.43; H, 4.63; N, 14.30.

[4,8-(2,2′-Biphenyldioxy)-16(or 17),23(or 24)-di-*tert*-butylphthalocyaninato(2−)]cobalt(II), AdCo4. A mixture of 2,2′-bis(2,3-dicyanophenoxy)biphenyl[3q] (311 mg, 7.09 × 10^{-4} mol), 4-*tert*-butylphthalonitrile (263 mg, 1.43 × 10^{-3} mol), cobalt dichloride (92 mg, 7.09 × 10^{-4} mol), and a catalytic amount of ammonium molybdate was refluxed in ethylene glycol (4 mL) for 5 h under nitrogen, and after cooling the residue was collected by filtration and washed with water and methanol. Alumina chromatography using hexane/chloroform (2:1 v/v) and subsequent recrystallization from ethyl acetate/hexane yielded 20 mg (3.3%) of a dark blue solid. Mass (FAB) (*m/z*): 866 (M$^+$). Anal. Found: C, 72.02; H, 5.09; N, 12.57. Calcd for C$_{52}$H$_{38}$N$_8$O$_2$-Co: C, 72.13; H, 4.42; N, 12.94.

[2^4,7^1-(2,2′-Biphenyldioxy)dibenzo[*b,g*]-12^3(or 12^4),17^3(or 17^4)-di-*tert*-butyldinaphtho[*l,q*]-5,10,15,20-tetraazaporphyrinato(2−)]cobalt(II), AdCo6. A mixture of 2,2′-bis(2,3-dicyanophenoxy)biphenyl[3q] (386 mg, 8.80 × 10^{-4} mol), 6-*tert*-butyldicyanonaphthalene[19] (444 mg, 1.89 × 10^{-3} mol), cobalt dichloride (131 mg, 1.01 × 10^{-3} mol), and a catalytic amount of ammonium molybdate was refluxed in ethylene glycol (4 mL) for 9 h under nitrogen, and after cooling the residue was collected by filtration and washed with water and methanol. Silica gel chromatography using toluene as eluent gave 12 mg (1.4%) of a green solid. Mass (FAB) (*m/z*): 966 (M$^+$). Anal. Found: C, 74.80; H, 5.04; N, 10.43. Calcd for C$_{60}$H$_{42}$N$_8$O$_2$Co: C, 74.60; H, 4.38; N, 11.60.

[2^4,7^1-(2,2′-Biphenyldioxy)dibenzo[*b,g*]-12^1,12^8,17^1,17^8-tetra(3-methylbutoxy)dianthro[*l,q*]-5,10,15,20-tetraazaporphyrinato(2−)]cobalt(II), AdCo8. 2,2′-Bis(2,3-dicyanophenoxy)biphenyl[3q] (111 mg, 2.53 × 10^{-4} mol) and 2,3-dicyano-1,4-diisopentoxyanthracene[3r] (205 mg, 5.12 × 10^{-4} mol) were dissolved in isoamyl alcohol (6 mL) containing lithium (5 mg, 7.2 × 10^{-4} mol), and the solution was refluxed for 1 h under nitrogen. After removal of half of the solvent by evaporation, DMF (4 mL) and cobalt dichloride (300 mg, 2.31 × 10^{-3} mol) were added, and the refluxing was continued for another hour. After addition of methanol and water, the solid product was collected by filtration and applied to silica gel chromatography using toluene as eluent. Recrystallization from hexane afforded 3.4 mg (1.0%) of the desired compound as a dark reddish brown solid. Mass (FAB) (*m/z*): 1298 (M$^+$). Anal. Found: C, 74.15; H, 5.89; N, 7.89. Calcd for C$_{80}$H$_{70}$N$_8$O$_6$Co: C, 74.00; H, 5.43; N, 8.63.

2^1,2^4,12^1,12^4-Tetraphenyldibenzo[*b,l*]-7,8,17,18-tetrapropyl-21*H*,23*H*-5,10,15,20-tetraazaporphyrin, OpH$_2$2. A mixture of dipropyl-fumaronitrile[21] (2 g, 1.23 × 10^{-3} mol), 3,6-diphenylphthalonitrile[16] (0.95 g, 3.38 × 10^{-3} mol), and lithium (100 mg, 1.44 × 10^{-2} mol) was refluxed in 1-pentanol for 80 min. After removal of the solvent by evaporation, the residue was imposed on a silica gel column using first toluene and then carbon tetrachloride as eluent. A portion of R_f = 0.25 was collected and washed well with hexane, to afford 96 mg (6.4%)

of the desired compound as a dark blue colored powder.[22] Mass (ESI-TOF) (*m/z*): 887 ([M + 1]$^+$). Anal. Found: C, 81.27; H, 6.32; N, 12.59. Calcd for C$_{60}$H$_{54}$N$_8$: C, 81.23; H, 6.14; N, 12.63. ^{1}H NMR (400 MHz, CDCl$_3$): δ −1.93 (br s, 2H, NH), 0.88 (t, 12H, CH$_3$), 1.72 (sextet, 8H, −CH$_2$−), 3.37 (t, 8H, CH$_2$−), 7.70 (m, 12H, phenyl *m*-, *p*-H), 7.91 (s, 4H, arom H), 8.08 (dd, 8H, phenyl *o*-H). UV−vis (*o*-DCB) λ_{max} (log ϵ): 335 (4.68), 570 (4.42), 613 (4.86), 683 (4.82).

[2^1,2^4,12^1,12^4-Tetraphenyldibenzo[*b*,*l*]-7,8,17,18-tetrapropyl-5,10,15,20-tetraazaporphyrinato(2−)]cobalt(II), OpCo2. OpH$_2$2 (10 mg, 1.12 × 10^{-5} mol) and Co(OAc)$_2$·4H$_2$O (160 mg, 6.42 × 10^{-4} mol) were refluxed in 2 mL of chlorobenzene/2-ethoxyethanol (1:1 v/v) at 140 °C for 3 h. After removal of the solvent by evaporation, the residue was purified by preparative TLC on silica using carbon tetrachloride/toluene (1:1 v/v) as eluent to give, after washing with hexane, 8 mg (75%) of the dark blue shiny desired solid. Mass (ESI-TOF) (*m/z*): 944 ([M + 1]$^+$). Anal. Found: C, 75.85; H, 5.52; N, 11.82. Calcd for C$_{60}$H$_{52}$N$_8$Co: C, 76.34; H, 5.55; N, 11.87.

2^1,2^4,12^1,12^4-Tetraphenyldibenzo[*b*,*l*]-7^2(or 7^3),17^2(or 17^3)-di-*tert*-butyldibenzo[*g*,*q*]-21*H*,23*H*-5,10,15,20-tetraazaporphyrin, OpH$_2$4. A mixture of 3,6-diphenylphthalonitrile[16] (2.8 g, 0.01 mol), 4-*tert*-butylphthalonitrile (1.84 g, 0.01 mol), and Zn(OAc)$_2$ (1.83 g, 0.01 mol) was heated at 200 °C for 8 h under nitrogen. The dark blue colored melt was treated in a refluxing acetic acid/hydrochloric acid (1:1 v/v) mixture (∼20 mL) for ca. 4 h. After cooling, the solution was poured onto crushed ice and neutralized with concentrated NH$_4$OH. The resultant dark blue solid was collected by filtration and washed with MeOH until the washings were colorless. The solid was then dissolved in CHCl$_3$ and purified by silica gel chromatography using CHCl$_3$/hexane (4:1 v/v) as eluent. The first blue fraction was collected and further purified by preparative TLC on silica using CHCl$_3$/hexane (4:1 v/v) as eluent, and subsequent recrystallization from CHCl$_3$/ethanol afforded 22 mg (0.47%) of the desired compound. Mass (MALDI-TOF) (*m/z*): 931 ([M + 1]$^+$). Anal. Found: C, 82.64; H, 5.64; N, 11.77. Calcd for C$_{64}$H$_{50}$N$_8$ (931.1576): C, 82.55; H, 5.41; N, 12.03. ^{1}H NMR (400 MHz, CDCl$_3$): δ −0.77, −0.58 (2s, 2H, NH), 1.68, 1.70 (2s, 18H, *t*-Bu), 7.76−8.63 (m, 30H, arom).

[2^1,2^4,12^1,12^4-Tetraphenyldibenzo[*b*,*l*]-7^2(or 7^3),17^2(or 17^3)-di-*tert*-butyldibenzo[*g*,*q*]-5,10,15,20-tetraazaporphyrinato(2−)]cobalt(II), OpCo4. OpH$_2$4 (9.3 mg, 0.01 mmol) and CoCl$_2$ 5.2 mg (0.04 mmol) were dissolved in dry DMF (∼10 mL), and the mixture was heated at 50 °C under nitrogen for 24 h. After evaporation of the DMF, the residue was dissolved in CHCl$_3$ and purified using preparative TLC and subsequent recrystallization from CHCl$_3$/ethanol to give 8.2 mg (77.3%) of the desired OpCo2. Mass (ESI-TOF) (*m/z*): 987 (M$^+$). Anal. Found: C, 75.87; H, 4.93; N, 11.15. Calcd for C$_{64}$H$_{48}$N$_8$Co·H$_2$O (1006.0902): C, 76.41; H, 5.01; N, 11.14.

2^1,2^4,12^1,12^4-Tetraphenyldibenzo[*b*,*l*]-7^3(or 7^4),17^3(or 17^4)-di-*tert*-butyldinaphtho[*g*,*q*]-21*H*,23*H*-5,10,15,20-tetraazaporphyrin, OpH$_2$6. Magnesium metal (0.24 g, 0.01 mol) and dry *n*-butyl alcohol (100 mL) were heated to reflux under nitrogen for 4 h, and 3,6-diphenylphthalonitrile[16] (2.8 g, 0.01 mol) and 6-*tert*-butyl-2,3-dicyanonaphthalene[19] (2.34 g, 0.01 mol) were added, and the reaction continued for 24 h. The solvent was removed using an evaporator, 50 mL of CF$_3$COOH was added, and the solution was stirred for ca. 15 min in the dark. The solution was poured onto crushed ice and neutralized with concentrated NH$_4$OH. The resultant dark green solid was filtered off and washed several times with MeOH until the washings became colorless. The solid was then purified by silica gel column chromatography using

CHCl$_3$/hexane (1:1 v/v) as eluent. The first green fraction was collected and further purified using preparative TLC on silica and the same eluent. The analytically pure sample was obtained by precipitation of the CHCl$_3$ solution using ethanol. Yield: 18 mg (0.35%). Mass (MALDI-TOF) (*m/z*): 1032 ([M + 1]$^+$). Anal. Found: C, 82.67; H, 5.43; N, 10.71. Calcd for C$_{72}$H$_{54}$N$_8$·H$_2$O (1049.293): C, 82.42; H, 5.38; N, 10.68. ^{1}H NMR (400 MHz, CDCl$_3$): δ −1.53 (br, 2H, NH), 1.71, 1.73 (2s, 18H, *t*-Bu), 7.47−8.64 (m, 34H, arom).

[2^1,2^4,12^1,12^4-Tetraphenyldibenzo[*b*,*l*]-7^3(or 7^4),17^3(or 17^4)-di-*tert*-butyldinaphtho[*g*,*q*]-5,10,15,20-tetraazaporphyrinato(2−)]cobalt(II), OpCo6. This compound was obtained by two methods. (i) A mixture of dry DMF (∼10 mL), OpH$_2$6 (10.3 mg, 0.01 mmol), and CoCl$_2$ (5.2 mg, 0.04 mmol) was heated at 50 °C under nitrogen for 24 h. After evaporation of the DMF, the residue was purified using preparative TLC with CHCl$_3$ as eluent, and further by reprecipitation from CHCl$_3$/ethanol, to give 7.6 mg (65.5%) of a green powder of the desired compound. Mass (ESI-TOF) (*m/z*): 1087 (M$^+$). Anal. Found: C, 77.23; H, 5.25; N, 11.00. Calcd for C$_{72}$H$_{52}$N$_8$Co·H$_2$O (1106.2102): C, 78.18; H, 4.92; N, 10.13. (ii) A mixture of 6-*tert*-butyl-2,3-dicyanonaphthalene[19] (300 mg, 1.28 × 10^{-3} mol), 3,6-diphenyl-phthalonitrile[16] (1.05 g, 3.74 × 10^{-3} mol), CoCl$_2$·2H$_2$O (139 mg, 8.38 × 10^{-4} mol), and a catalytic amount of ammonium molybdate was mixed well and heated at 195 °C for 8 h in ethylene glycol (6 mL). After the mixture cooled, methanol was added and the resultant precipitate collected, washed with methanol, and imposed on an alumina column using toluene as eluent. The fifth blue band was collected and further purified by silica gel chromatography using toluene as eluent (R_f = 0.65) and crystallized from chloroform/methanol to give 11 mg (1.6%) of a green powder of the desired compound. Mass (FAB) (*m/z*): 1088 ([M + 1]$^+$). Anal. Found: C, 79.00; H, 5.02; N, 10.14. Calcd for C$_{72}$H$_{52}$N$_8$Co (1088.1947): C, 79.47; H, 4.82; N, 10.30.

[2^1,2^4,12^1,12^4-Tetraphenyldibenzo[*b*,*l*]-7^4(or 7^5),17^4(or 17^5)-di-*tert*-butyldianthro[*g*,*q*]-5,10,15,20-tetraazaporphyrinato(2−)]cobalt(II), OpCo8. 3,6-Diphenylphthalonitrile[16] (620 mg, 2.21 × 10^{-3} mol), 6-*tert*-butyl-2,3-dicyanoanthracene[17b,20] (210 mg, 7.38 × 10^{-4} mol), CoCl$_2$·2H$_2$O (110 mg, 7.33 × 10^{-4} mol), and a catalytic amount of ammonium molybdate were mixed well in an agate mortar and charged in a pressure-proof cylinder. After the reaction proceeded for 40 min at 270 °C, the products were imposed on an alumina column using first CH$_2$Cl$_2$ until all the soluble material came out and then CH$_2$Cl$_2$/MeOH to elute the portion containing the desired compound. The latter portion was further purified using preparative TLC on silica and toluene containing 2% pyridine (R_f = 0.72), and further using preparative TLC on alumina with CHCl$_3$ as eluent (R_f = 0.5), to give 1.4 mg (0.3%) of green powder of the desired compound. Mass (FAB) (*m/z*): 1188 (M$^+$).

Results and Discussion

(i) Synthesis. The synthesis of the adjacently substituted species was straightforward. By the use of diphthalonitrile linked by the shortest linkage, i.e., 2,2′-bis(2,3-dicyanophenoxy)-biphenyl,[3q] the desired compounds were obtained without danger of contamination by opposite species. However, in the case of the opposite type species, it was necessary to confirm the D_{2h} type structure before insertion of the cobalt. The reactivity for cyclization of the aromatic ortho dinitriles decreased the larger the π system. Accordingly, to obtain larger macrocycles, more severe reaction conditions (higher reaction temperatures and longer reaction times) were required, yet the yields were not increased markedly. In addition, purification of the larger complexes became harder due to their reduced solubility and stronger adsorption to silica or alumina columns. The stability also seemed to be decreased for larger macrocycles. For example, although OpCo6 and OpCo8 were stable in the solid state, the color of an *o*-DCB solution of OpCo6 and OpCo8 changed gradually over a period of days.

(22) A portion with R_f = 0.15 (silica, CCl$_4$) was confirmed to be the corresponding adjacent isomer, 2^1,2^4,7^1,7^4-tetraphenyldibenzo[*b*,*g*]-12,13,-17,18-tetrapropyl-21*H*,23*H*-5,10,15,20-tetraazaporphine, from the following data. Mass (ESI-TOF) (*m/z*): 887 ([M + 1]$^+$). ^{1}H NMR (400 MHz, CDCl$_3$): δ −0.32, −0.35 (2s, 2H, NH), 0.88 (t, 6H, CH$_3$), 1.22 (t, 6H, CH$_3$), 1.68 (sextet, 4H, −CH$_2$−), 2.23 (sextet, 4H, −CH$_2$−), 3.27 (t, 4H, CH$_2$−), 3.71 (t, 4H, CH$_2$−), 7.23−7.41 (m, 8H, phenyl), 7.70−7.74 (m, 8H, phenyl), 7.83 (d, 2H, arom H), 7.93 (d, 2H, arom H), 8.11 (dd, 4H, phenyl). UV−vis (CHCl$_3$) λ_{max}: 269, 333, 586, 642, 685.
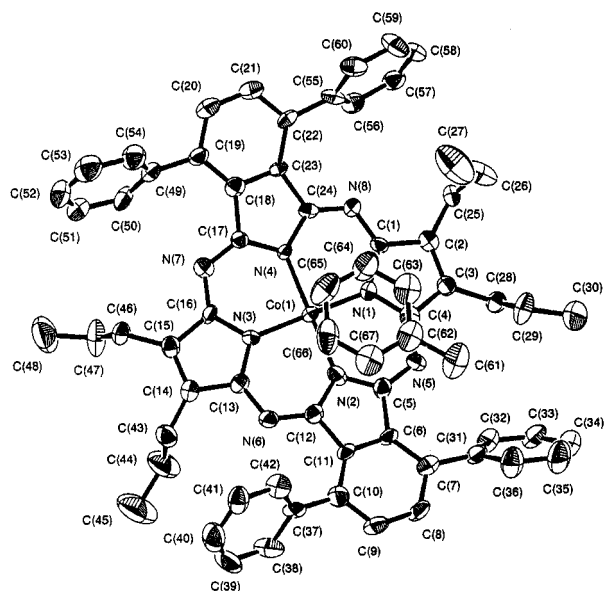
Figure 2. ORTEP drawing of OpCo2·C$_6$H$_5$CH$_3$ showing the 50% probability thermal ellipsoids. Hydrogen atoms have been omitted for clarity.

(ii) X-ray Crystal Analysis of OpCo2. Although the D_{2h} structure was confirmed in most cases from measurements of ^{1}H NMR and electronic absorption spectra, the structure of OpCo2 was also confirmed by X-ray analysis of a single crystal which was grown from toluene/methanol solution, since it gave an unusual electronic spectrum (see following sections). The crystal data and experimental details are summarized in Table 1. As shown in Figure 2, OpCo2 had the expected opposite type D_{2h} π structure.[23] The X-ray structural data for the same π structure were previously reported for a nickel complex.[3g] In that case, all bond lengths and angles within the two distinct types of pyrroles were nearly equivalent. In OpCo2, the Cα−Np−Cα angles in pyrroles with the fused benzo rings (108.1(7)° and 106.8(8)°) are slightly larger than those in the alkyl-linked

Table 1. Crystal Data and Experimental Details of OpCo2

empirical formula	C$_{67}$H$_{60}$N$_8$Co
formula weight	1036.20
crystal system	triclinic
space group	$P\bar{1}$ (No. 2)
crystal color, habit	blue, plate
crystal dimensions	0.05 × 0.10 × 0.20 mm
lattice parameters	$a = 12.890(2)$ Å
	$b = 14.5300(8)$ Å
	$c = 16.270(4)$ Å
	$\alpha = 69.290(8)°$
	$\beta = 69.750(4)°$
	$\gamma = 84.370(4)°$
	$V = 2673.1(8)$ Å^3
temperature	−100.0 °C
Z value	2
residuals: $R1$; Rw	0.070; 0.103
goodness-of-fit indicator	1.25
linear absorption coefficient	3.72 cm^{-1}

pyrroles (106.4(8)° and 105.1(8)°), and the Co−N(pyrrole) distance along the long axis of the molecule (av. 1.92 Å) is longer by 0.01 Å than that along the short axis. Although not explicitly perceivable in Figure 2, the plane connecting the two fused benzo rings is slightly bent toward a toluene molecule included in the crystal (for further details, see Supporting Information).

(iii) Electronic Absorption and Magnetic Circular Dichroism Spectroscopy. We could not detect any evidence for aggregation until ca. 10^{-4} mol/L. Accordingly, spectroscopic data were collected at concentrations lower than this concentration.

(a) C_{2v} Species. Figure 3A and B shows absorption and MCD spectra, respectively, of C_{2v} species in toluene, with the Q-band data for these summarized in Table 2. With increasing size of the π system, the Q-band shows a significant shift to longer wavelength, while the Soret band broadens and has a slight shift to longer wavelength. The shifts of the Q-bands are 1550 cm^{-1} for Co0−AdCo2, 1020 cm^{-1} for AdCo2−AdCo4, 837 cm^{-1}
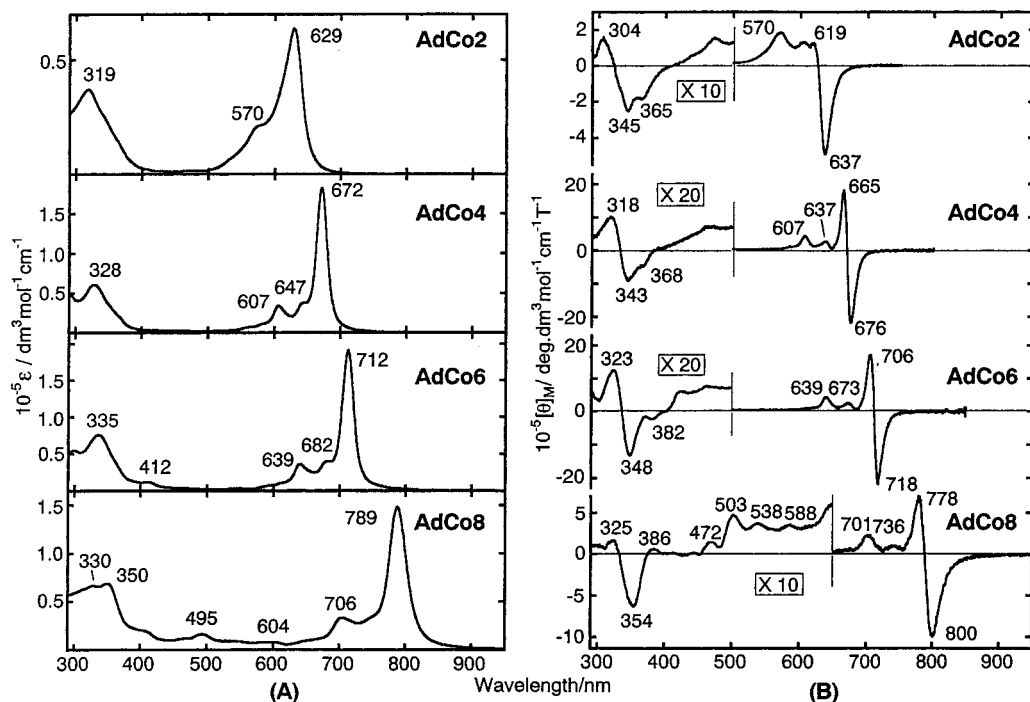

Figure 3. (A) Electronic absorption and (B) MCD spectra of Co0, AdCo2, AdCo4, AdCo6, and AdCo8 in toluene.

Table 2. Electronic Absorption and MCD Spectral Data

species	electronic absorption λ/nm (log ϵ)				MCD λ/nm ($10^{-4}[\theta]_M$/deg·dm³ mol⁻¹ cm⁻¹ T⁻¹)				long/short[a]	$\Delta\lambda$/cm⁻¹ [b]	f [c]
Co0	319 (4.47)	338 (4.46)	573 (4.59)		321 (−1.45) 580 (−21.3)	348 (−2.33)	526 (12.0)	560 (12.6)	1.00	0	0.012
AdCo2	319 (4.57)	570 (4.32)	629 (4.80)		304 (1.89) 619 (12.9)	345 (−2.49) 637 (−49.4)	365 (−1.82)	570 (18.7)	1.00	∼0	0.129
AdCo4	328 (4.78)	607 (4.53)	647 (4.58)	672 (5.26)	318 (5.09) 665 (181)	343 (−4.59) 676 (−218)	607 (44.6)	637 (26.8)	1.00	199	0.193
AdCo6	335 (4.87) 712 (5.28)	412 (4.05)	639 (4.56)	682 (4.60)	323 (6.25) 639 (43.0)	347 (−6.66) 673 (25.5)	382 (−1.18) 706 (171)	424 (3.07) 718 (−219)	1.00	269	0.234
AdCo8	330 (4.82)	350 (4.84) 789 (5.17)	495 (4.20)	706 (4.52)	325 (1.68) 702 (22.8)	354 (−6.37) 739 (10.4)	472 (1.46) 779 (70.3)	504 (4.74) 801 (−100)	1.00	274	0.240
OpCo2	328 (4.76)	583 (4.45)	639 (4.92)		308 (1.52) 630 (23.0)	340 (−4.40) 654 (−45.4)	364 (−3.23)	582 (19.5)	1.62	545	
OpCo4	331 (4.86)	610 (4.47)	673 (5.01)	697 (5.01)	323 (3.02) 698 (−83.3)	347 (−6.89)	618 (26.4)	668 (35.1)	1.00	602	
OpCo6	323 (4.86) 763 (4.96)	631 (4.53)	688 (4.95)	705 (4.89)	323 (3.09) 705 (5.56)	352 (−5.79) 762 (−48.6)	632 (17.5)	680 (50.1)	1.37	1025	
OpCo8	323 (4.85) 825 (4.67)	372 (4.76)	658 (4.49)	719 (4.89)	316 (1.92) 712 (28.4)	368 (−4.69) 826 (−22.5)	417 (−1.82)	474 (1.92)	1.73	1884	

[a] Geometrical ratio of the long axis to short axes of π conjugated structures. [b] Splitting of the Q-band estimated by band deconvolution analysis of both electronic absorption and MCD spectral data. [c] The oscillator strength of the Q-band estimated by band deconvolution analysis.

for AdCo4−AdCo6, and 1370 cm⁻¹ for AdCo6−AdCo8. Here, the substituent effect must be taken into account, particularly since the effect of the alkoxy group is large when it is linked to the benzene periphery closest to the Pc core (the so-called α positions).[24,25] Substituent effects depend on the type and number of the substituent groups, and approximate additivity exists when the same substituent is introduced at the same position of fused aromatics. For example, when the Q-band of tetra-*tert*-butylated ZnPc prepared from 4-*tert*-butylphthalonitrile is compared with that of peripherally unsubstituted ZnPc, the Q-band of the former occurs at longer wavelength than the latter, by ca. 140 cm⁻¹ (i.e., 33 cm⁻¹ per *tert*-butyl group).[26] Similarly, the Q-band position of Pc's containing eight alkoxy groups at the so-called α positions appears approximately 1400−1840 cm⁻¹ lower in energy than the band position of unsubstituted species.[25,27] Thus, if we unify the substituent effect, calculating from the effect of *tert*-butyl groups and alkoxy groups, the above differences may be ca. 1320, 1020, 837, and 520−740 cm⁻¹, respectively, in the above order, i.e., per two benzene units. The shift is, in this way, not linear with respect to the number of fused benzene unit, but its extent decreases with increasing molecular size. In other words, the substituent effect of the outer benzene unit is smaller than that of the inner one. Thus, when a benzene unit is fused to the tetraazaporphyrin (TAP) skeleton directly, the wavelength of the Q-band shift is roughly ca. 510−660 cm⁻¹, while for a benzene unit fused via benzene and naphthalene, it is approximately 420 and 260−370 cm⁻¹, respectively. This is also seen when comparing the Q-band position between AdCo8 (789 nm, 12 670 cm⁻¹) and tetra-*tert*-butylated cobalt naphthalocyanine (756 nm, 13 230 cm⁻¹)[24] in the same solvent. The size of the π conjugation system of both compounds is the same; i.e., eight benzene units are fused to the TAP skeleton. If we eliminate the substituent effect of the *tert*-butyl and alkoxy groups, the Q_{00}-band of these compounds may appear at around 735 ± 6 and 752 ± 1 nm (ca. 13 600 ± 100 and 13 300 cm⁻¹),[24] respectively. Thus, although the π skeleton of AdCo8 (adjacently dinaphtho-substituted Pc) and naphthalocyanine has an isomeric relationship, the effective π size of the former appears smaller. This is again reasonably

interpreted if we consider that the substituent effect of the outer fused benzene unit is smaller than that on the inner side.[3r]

A few small absorption peaks have been detected between the Q and Soret bands of AdCo6 and AdCo8 (Figure 3A). These are assigned to transitions restricted mainly in the naphthalene or anthracene ring moieties (see MO section).

The MCD spectra of these C_{2v} (D_{4h} for Co0) species show dispersion type, Faraday *A*-term type curves corresponding to the Q_{00} absorption peaks, indicating that their excited states are orbitally doubly degenerate.[28] The occurrence of this phenomenon for C_{2v} type species, however, was predicted ca. 40 years ago independently by Ballhausen[29a] and Gouterman.[29b] When benzene units are fused to the D_{4h} TAP skeleton, viewing radially from the center of the TAP skeleton, the originally degenerate Q_{x00} and Q_{y00} bands shift to longer wavelength to the same extent, so that a single Q-band without detectable energy splitting is observed even in the resultant C_{2v} type compounds. The appearance of Faraday *A*-term type curves in a system lacking a symmetry element higher than a 3-fold rotation axis may be surprising. However, if the Q_{x00} and Q_{y00} bands differ slightly in energy, these Faraday *A*-term type curves can be rationalized as pseudo *A*-terms[30a] produced by the superimposition of closely lying Faraday *B*-terms of opposite signs.[30b] The SAP effect is a first-order perturbation.[4,29b] Accordingly, the Q-band position of the Q_{x00} and Q_{y00} bands in C_{2v} π systems is expected to be at the same energy. Later, however, we show that MO calculations based on the actual C_{2v} symmetry and including much higher perturbation terms than the SAP method produce a slightly split Q-band (section (v)).

To understand the spectroscopic variations more quantitatively, the oscillator strength, f, of the Q-band was estimated

(23) Detailed X-ray data are available as Supporting Information.

(24) Luk'yanets, E. A. *Electronic Spectra of Phthalocyanines and Related Compounds*; NIOPIK: Moscow, 1989.
(25) (a) Kobayashi, N.; Sasaki, N.; Higashi, Y.; Osa, T. *Inorg. Chem.* **1995**, *34*, 1636. (b) Cook, M. J.; Dunn, A. J.; Howe, S. D.; Thomson, A. J.; Harrison, K. J. *J. Chem. Soc., Perkin Trans. 1* **1998**, 2453. (c) Bedworth, P. V.; Perry, J. W.; Marder, S. R. *Chem. Commun.* **1997**, 1353.
(26) Konami, H.; Hatano, M. *Chem. Lett.* **1988**, 1359.
(27) Our unpublished data.
(28) Stillman, M. J.; Nyokong, T. In ref 1, Vol. 1, Chapter 3.
(29) (a) Ballhausen, C. J. *Introduction to Ligand Field Theory*; McGraw-Hill: New York, 1962. (b) Gouterman, M. *J. Mol. Spectrosc.* **1961**, *6*, 138.
(30) (a) Kaito, A.; Nozawa, T.; Yamamoto, T.; Hatano, M.; Orii, Y. *Chem. Phys. Lett.* **1977**, *52*, 154. (b) Tajiri, A.; Winkler, Z. *Z. Naturforsch.* **1983**, *38a*, 1263.
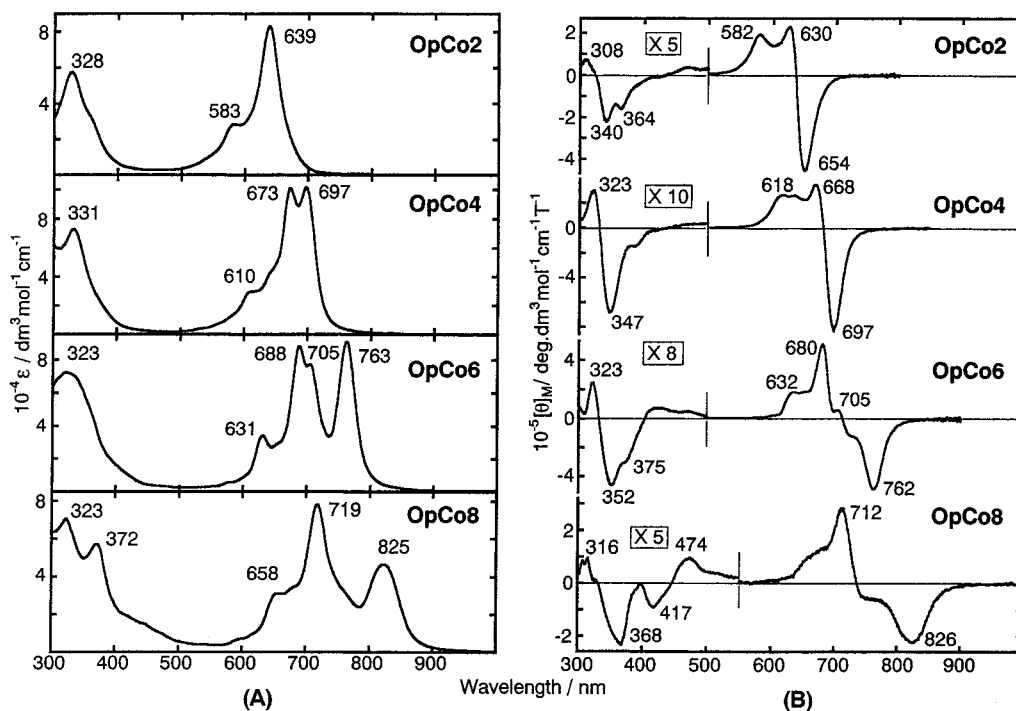
Figure 4. (A) Electronic absorption and (B) MCD spectra of OpCo2, OpCo4, OpCo6, and OpCo8 in *o*-DCB.

by band deconvolution analysis (Table 2).[31,32] The value is seen to increase, while the extent of the change decreases with increasing molecular size.

(b) D_{2h} Species. Figure 4A and B displays absorption and MCD spectra of D_{2h} type species in toluene, with data summarized in Table 2. Only OpCo2 was prepared from 3,6-diphenylphthalonitrile and dipropylmaleonitrile, since when *tert*-butylated maleonitrile was used as one of the two starting dinitriles, the desired compound could not be separated from the other reaction products. However, since the substituent effect of alkyl groups is small,[24,26] we considered that this would not produce any serious problem for the analysis and discussion. Similarly to the case for the above C_{2v} type species, the Q-band shifts to longer wavelength, while the extent of change decreases with increasing molecular size. In addition, the Q-band generally splits into two peaks, and the degree of splitting increases with increasing molecular size. If we define the center of the split bands as the band position, ΔE of OpCo2−OpCo4, OpCo4−OpCo6, and OpCo6−OpCo8 are 1050, 960, and 631 cm^{-1}, respectively, and the splitting energies of the Q-bands change as summarized in Table 2. Compared with the Q-band, the Soret band position does not change significantly from species to species and remains in the 323−328 nm region. The peak at 372 nm of OpCo8 may be a split component of the Soret band, since the MCD spectra give opposite signs corresponding to the absorption peaks at 323 and 372 nm.

The MCD spectra of these species are composed of super-position of Faraday *B*-terms, since there is no orbital degeneracy

in these molecules. The Q MCD bands of OpCo2 and OpCo4 look like Faraday *A*-terms in shape, but these are produced by the superimposition of closely lying Faraday *B*-terms of opposite signs.[30] The energy difference between the opposite and adjacent isomers increases with increasing ratio of long axis to short axis, and in the cases of Co8 species, the splitting energies for the opposite and adjacent isomers become 1940 and 353 cm^{-1}, respectively. In the spectra of OpCo4, OpCo6, and OpCo8, the positions of the MCD peaks and troughs nearly correspond to the absorption peaks, supporting the contribution of Faraday *B*-terms.

(iv) Electrochemistry and Spectroelectrochemistry. Cyclic voltammograms of all the cobalt complexes are shown in Figure 5, and the electrochemical data are summarized in Table 3. Although the substituent groups of the adjacently and oppositely substituted complexes are different, there are many similarities between the complexes. For example, the potentials of the first reduction (Co$^{II/I}$) and second reduction couples (ligand first reduction, $L^{-2/-3}$) are very close to each other for all complexes, indicating that the orbital energy for accepting electrons (d$_{z^2}$ and the LUMO) does not change significantly from species to species, even if the size of the molecule varies. Another similarity is the significant negative shift of the first ($L^{-1/-2}$) and second ligand oxidation ($L^{0/-1}$) potentials with increasing molecular size (Table 3). Thus, irrespective of the molecular shape, whether it is C_{2v} or D_{2h}, the HOMO destabilizes with increasing molecular size.[33] However, there are also some differences. We observed two characteristics. The most notable difference was seen in the cyclic voltammograms of AdCo2

(31) Band deconvolution of the spectral data was carried out using the program SIMPFIT developed by Stillman's group.[32] Reasonable fits could be obtained by fitting Faraday *A*-terms at the Q-bands of these compounds. Detailed band fitting parameters are available as Supporting Information.

(32) (a) Browett, W. R.; Stillman, M. J. *Comput. Chem.* **1987**, *11*, 241. (b) Nyokong, T.; Gasyna, Z.; Stillman, M. J. *Inorg. Chem.* **1987**, *26*, 1087. (c) Browett, W. R.; Gasyna, Z.; Stillman, M. J. *J. Am. Chem. Soc.* **1988**, *110*, 3633. (d) Ough, E.; Nyokong, T.; Creber, K. A. M.; Stillman, M. J. *Inorg. Chem.* **1988**, *27*, 2724. (e) Ough, E. A.; Stillman, M. J. *Inorg. Chem.* **1994**, *33*, 573. (f) Mack, J.; Stillman, M. J. *J. Am. Chem. Soc.* **1994**, *116*, 1292.

(33) Concerning the argument of the changes of the HOMO energies based upon redox potential shifts, one reviewer pointed out that the shifts may reflect large changes in stabilization energies of the oxidized rather than parent species. This possibility cannot be ruled out. However, we feel that the shifts are more related to the changes of the HOMO energies as follows. Namely, if we can presume that the larger compounds are more readily oxidized by allowing the positive charge to be delocalized to a larger extent, the shifts of the LUMO also can be conjectured to change in a similar manner. The experimental results, however, do not show this trend.
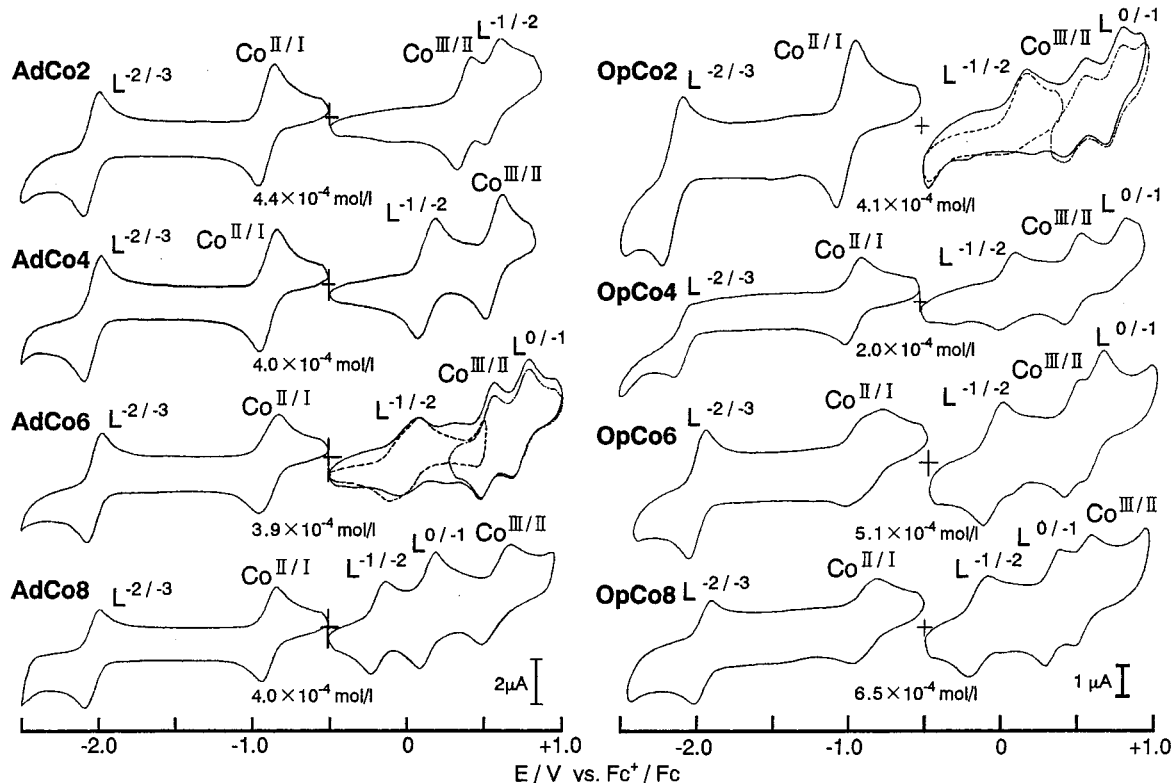
Figure 5. Cyclic voltammograms of all cobalt complexes in this study, measured at a scan rate of 50 mV/s in *o*-DCB containing 0.1 M TBAP. Concentrations of the compounds used for the measurements are shown.

Table 3. Redox Potential Data (vs Fc[+]/Fc) for AdCo2, AdCo4, AdCo6, AdCo8, OpCo2, OpCo4, OpCo6, and OpCo8 in *o*-Dichlorobenzene Containing 0.1 M TBAP[a]

species	$E^{3+/2+}$ ($L^{0/-1}$)	$E^{2+/1+}$ (Co[III/II])	$E^{1+/0}$ ($L^{-1/-2}$)	$E^{0/1-}$ (Co[II/I])	$E^{1-/2-}$ ($L^{-2/-3}$)	$\Delta E_p{}^b$
AdCo2		0.40 (0.10)	0.58 (0.10)	−0.89 (0.11)	−2.03 (0.11)	2.61
AdCo4		0.60 (0.11)	0.16 (0.12)	−0.87 (0.10)	−2.02 (0.12)	2.18
AdCo6	0.75 (0.11)	0.54 (0.11)	0.03 (0.20)	−0.89 (0.10)	−2.02 (0.10)	2.05
AdCo8	0.17 (0.10)	0.61 (0.20)	−0.15 (0.10)	−0.86 (0.10)	−2.01 (0.10)	1.86
OpCo2	0.73 (0.11)	0.48 (0.14)	0.14, 0.25[c]	−1.03 (0.12)	−2.17 (0.14)	2.42
OpCo4	0.76[c]	0.48 (0.11)	0.05 (0.10)	−0.97 (0.10)	−2.03[c]	2.08
OpCo6	0.62 (0.10)	0.48 (0.10)	−0.05 (0.13)	−0.90 (0.22)	−2.00 (0.10)	1.95
OpCo8	0.34 (0.09)	0.54 (0.10)	−0.14 (0.13)	−0.90 (0.15)	−1.97 (0.11)	1.83

[a] Numbers in parentheses indicate the potential differences between negative and positive peak potentials at a sweep rate 50 mV/s. [b] The potential differences between the first oxidation and reduction potentials. [c] The potentials are not clear in the cyclic voltammograms, therefore, these potentials are determined from differential pulse voltammograms.

and OpCo2 in the positive potential region. Although the assignment of the redox couple was based on the spectroelectrochemistry results, which are described below, the first oxidation couple for AdCo2 is assigned to the Co[III/II] couple, while that for OpCo2 is assigned to the first ligand oxidation. Because of this phenomenon, there is a possibility that the first ligand oxidation potential of AdCo2 is more positive than that of normal AdMt2 without metal oxidation, since part of the +1 charge of cobalt spreads over the ligand, thereby making ligand oxidation more difficult. The second point concerns the detection of the second ligand oxidation couple. As seen in the voltammograms, this couple is observed for all oppositely substituted species, but in the case of adjacently substituted species it is only seen with naphthalene and anthracene substituted species. This may be related to the fact that the Q-band position of AdCo species lies at shorter wavelength than the longest wavelength component of the split Q-band of OpCo species.

Oxidation across the first couple of AdCo2 and OpCo2 resulted in the spectroscopic changes shown in Figure 6A and B, respectively. In the case of AdCo2, the Soret band decreased in intensity and a new peak appeared to longer wavelength, while the Q-band intensified markedly, with isosbestic points occurring at five wavelengths. These are the changes commonly observed when Co[II] is oxidized to Co[III] species in Pc and Pc analogues.[34] Although the first oxidation of CoPc occurs at the cobalt in coordinating solvents such as DMF, it generally occurs at the ligand in noncoordinating solvents such as *o*-DCB, as used in this study. AdCo2 is only the second example of a compound showing the first oxidation at cobalt in noncoordinating solvent, following tetra-*tert*-butylated tetraazaporphyrin.[17a] Since the first oxidation of cobalt tetraphenyl- and octaeth-

(34) (a) Nevin, W. A.; Liu, W.; Greenberg, S.; Hempstead, M. R.; Marcuccio, S. M.; Melnik, M.; Leznoff, C. C.; Lever, A. B. P. *Inorg. Chem.* **1987**, *26*, 891. (b) Kobayashi, N.; Herman, L. W.; Nevin, W. A.; Janda, P.; Leznoff, C. C.; Lever, A. B. P. *Inorg. Chem.* **1990**, *29*, 3415. (c) Day, P.; Hill, H. A. O.; Price, M. G. *J. Chem. Soc. (A)* **1968**, 90.
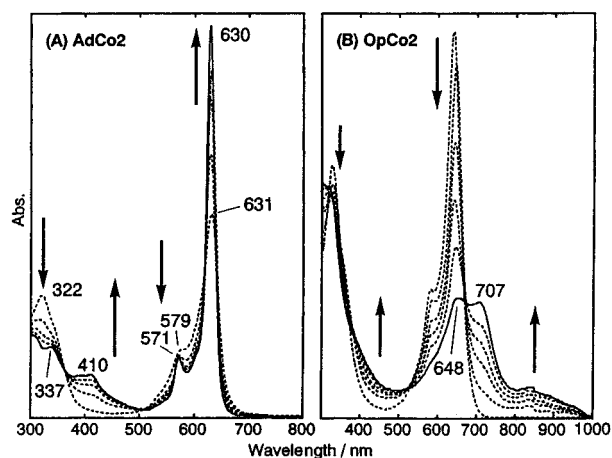
Figure 6. Development of the electronic spectra of (A) AdCo^{II}2 and (B) OpCo^{II}2 with time, showing the formation of (A) cobalt-oxidized AdCo^{III}2 and (B) ligand-oxidized OpCo^{II}2 radical species, respectively. The applied potentials were +0.96 and +0.82 V vs Ag/AgCl, respectively.

Figure 7. Development of the electronic spectra of (A) AdCo^{II}2 and (B) OpCo^{II}2 with time, showing the formation of cobalt-reduced (A) AdCo^{I}2 and (B) OpCo^{I}2, respectively. The applied potentials were −1.0 and −1.3 V vs Ag/AgCl, respectively.

ylporphyrins in noncoordinating solvents generally occurs at cobalt, AdCo2 appears to be intermediate between normal porphyrins and Pc's.[35] In contrast, in the spectra of OpCo2, the original Q-band decreased in intensity, and a new Q-band peak developed at longer wavelength, at 707 nm, together with a weak, broad band extending to ca. 1000 nm. These are indications of ligand oxidation, which is seen not only in cobalt Pc's but also in other metallo Pc's.[36] Thus, OpCo^{II}2 was concluded to be oxidized to OpCo^{II}2 ring-oxidized cation radical species.

Although not shown, when the AdCo^{III}2 species was further oxidized at a potential positive of the second oxidation potential (+1.2 V vs Ag/AgCl), the intense Q-band decreased in intensity and a new peak appeared at a longer wavelength, 668 nm, together with a small peak at ca. 950 nm. From these changes, we concluded that the ligand was oxidized[36] to produce the AdCo^{III}2 π cation radical species.

Figure 7A and B shows the spectroscopic changes observed across the first reduction of AdCo2 and OpCo2, respectively. With the progress of electrolysis, both compounds showed roughly similar changes; the Q-band faded away and a new Q-band, which has approximately half the intensity of the original Q-band, developed at longer wavelength, accompanied by an increase in absorbance in the region between the Q and Soret bands. A set of isosbestic points was detected at least at three wavelengths. These are similar to the changes observed to date for many CoPc derivatives when Co^{II} was reduced to Co^{I}, and the band developed between the Q and Soret bands has been assigned to an MLCT band from cobalt e$_g$ to ligand b$_{1u}$ and b$_{2u}$ orbitals under D$_{4h}$ symmetry.[37] Thus, there is no doubt that the first reduction is occurring at cobalt.

The size and symmetry dependence of the first and second oxidation and the first reduction couples is summarized in Figure 8, collected from the data in Figure 5 and Table 3. This figure demonstrates that there are a few differences between the
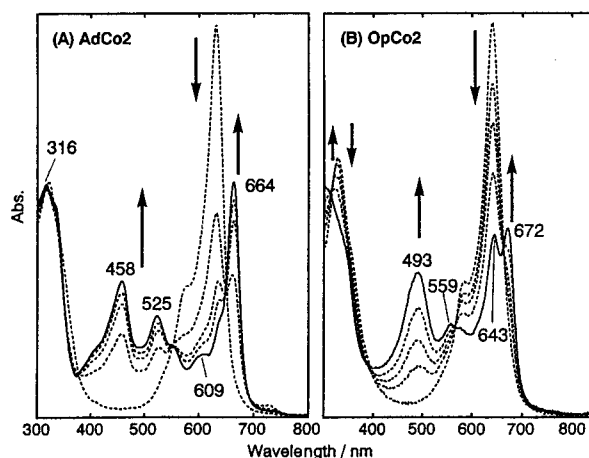
(35) Wolberg, A.; Manassen, J. *J. Am. Chem. Soc.* **1970**, *92*, 2982. Lin, X. Q.; Kadish, K. M. *Anal. Chem.* **1985**, *57*, 1498.
(36) Manivannan, V.; Nevin, W. A.; Leznoff, C. C.; Lever, A. B. P. *J. Coord. Chem.* **1988**, *19*, 139. Stillman, M. J. In ref 1, Vol. 3, Chapter 5. Nevin, W. A.; Lever, A. B. P. *Anal. Chem.* **1988**, *60*, 727.
(37) Stillman, M. J.; Thomson, A. J. *J. Chem. Soc., Faraday Trans. 2* **1973**, *70*, 790. Kobayashi, N. *Coord. Chem. Rev.* **2001**, *219−221*, 93.
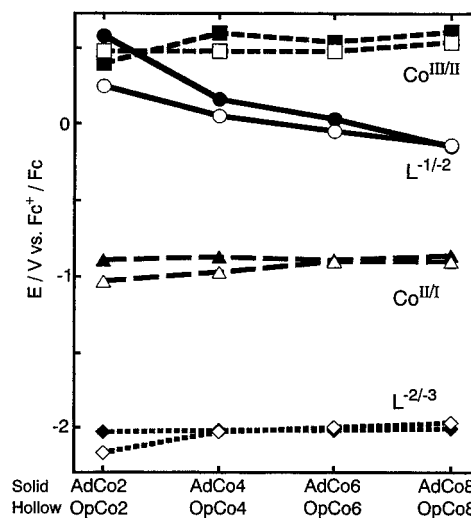
Figure 8. Size and symmetry dependence of the first and second oxidation and the first reduction couples, for data collected from Figure 5 and Table 3.

opposite and adjacent isomers. For example, although the first reduction potential of adjacent species is independent of the molecular size, that of the oppositely substituted species stabilizes slightly with increasing molecular size. Although the extent of this is only slight, it appears to be real, since the first reduction potential shifts systematically positively with increasing molecular size. This may be related to the splitting of the LUMO in the oppositely substituted species, since the LUMO energy in these species is always lower than that of the core. In addition, although not easily perceivable from this figure, the potential difference between the first oxidation and reduction of oppositely substituted species is approximately 100 mV smaller than that in the adjacently substituted species.

(v) Molecular Orbital Calculations. (a) Predicted Absorption Spectra. To enhance our understanding of the above spectroscopic and electrochemical data, MO calculations have been performed using the ZINDO/S Hamiltonian.[12] Figure 9A and B displays the calculated spectra, while Table 4 summarizes the details of the calculation results, including orientation of transition dipoles and configurations. Calculations were carried out for the zinc structures, since Co(II) is paramagnetic.

Table 4. Calculated Transition Energies, Oscillator Strength (*f*), and Configurations[a]

energy/cm⁻¹	nm	f	pol.[b]	configurations[c]			energy/cm⁻¹	nm	f	pol.[b]	configurations[c]		
TAP													
16330	612	0.656	x	57−58 (89)			35010	286	0.061	x	55−59 (92)		
16330	612	0.656	y	57−59 (89)			36150	277	2.806	y	56−58 (84)	57−59 (10)	
35010	286	0.061	y	55−58 (92)			36150	277	2.806	x	56−59 (84)	57−58 (10)	
AdZn2													
15540	644	0.753	y	75−76 (95)			36880	271	0.272	y	73−76 (81)		
15610	640	0.863	x	75−77 (93)			37090	270	0.208	x	72−76 (57)	71−77 (11)	
27480	364	0.051	y	75−79 (95)			37100	270	0.357	y	75−83 (46)	71−76 (21)	
35210	284	0.999	y	74−77 (48)	72−77 (29)		38690	258	0.467	y	75−81 (37)		
36140	277	0.341	y	71−76 (27)	75−81 (16)		39300	254	0.139	y	75−81 (29)	75−83 (28)	
36270	276	2.27	x	74−76 (68)	72−76 (15)								
AdZn6													
13370	748	1.123	y	111−112 (95)			36530	274	0.15	x	111−122 (75)		
13460	743	1.199	x	111−113 (95)			36850	271	1.404	y	108−113 (55)	104−113 (16)	
19720	507	0.074	y	111−114 (95)			37800	265	0.405	y	107−112 (20)	105−112 (17)	
31450	318	0.167	x	110−120 (82)			38320	261	0.289	x	111−124 (58)		
32020	312	0.148	y	110−113 (49)	109−112 (23)		38360	261	0.36	y	107−112 (36)	111−125 (26)	
34240	292	0.08	x	111−120 (66)	109−113 (19)		38800	258	0.231	x	107−113 (27)	111−124 (19)	104−112 (15)
35830	279	0.495	y	111−123 (70)			39860	251	0.145	x	106−112 (36)		
36470	274	1.94	x	108−112 (65)			40090	249	0.432	x	110−114 (23)	104−112 (19)	109−115 (16)
AdZn8													
12760	783	1.102	y	129−130 (95)			33740	296	0.078	y	128−133 (38)	127−132 (22)	
13060	766	1.282	x	129−131 (95)			35590	281	0.81	y	129−141 (39)	129−142 (38)	
17820	561	0.178	y	129−132 (93)			35740	280	2.423	x	126−130 (37)		
19060	525	0.056	x	129−133 (95)			36230	276	0.619	y	129−141 (26)	129−145 (25)	126−131 (22)
27550	363	0.064	x	128−130 (8)			36550	274	1.443	y	126−131 (32)	129−142 (22)	
28660	349	0.11	y	128−131 (66)			37220	269	0.176	x	123−131 (58)		
28960	345	0.213	y	127−130 (37)	129−137 (26)		37730	265	0.263	x	129−143 (30)	129−144 (30)	
29360	341	0.266	y	127−131 (55)	128−132 (21)		37830	264	0.258	y	123−130 (39)		
33460	299	0.06	x	129−140 (43)			38630	259	0.512	x	126−130 (22)		
Nc													
12740	785	1.301	x	129−130 (95)			35230	284	0.148	y	125−131 (40)		
12740	785	1.301	y	129−131 (95)			36190	276	0.227	y	129−142 (50)	129−143(22)	
21300	469	0.09	x	129−134 (90)			36190	276	0.227	x	129−143 (50)	129−142 (22)	
21300	469	0.09	y	129−135 (90)			36930	271	2.6 16	y	124−130 (56)	125−131 (29)	
31960	313	0.204	x	128−130 (71)			36930	271	2.616	x	124−131 (56)	125−130 (29)	
31960	313	0.204	y	128−131 (71)			39120	256	0.466	y	123−130 (70)		
35230	284	0.148	x	125−130 (40)			39120	256	0.466	x	123−131 (70)		
Pc													
14240	702	1.071	y	93−95 (91)			37580	266	0.807	y	92−94 (48)	93−102 (26)	89−94 (15)
14240	702	1.071	x	93−94 (91)			37580	266	0.807	x	92−95 (48)	93−103 (26)	89−95 (15)
36020	278	0.985	y	93−102 (68)	92−94 (22)		38290	261	0.866	y	89−94 (73)	92−94 (19)	
36020	278	0.985	x	93−103 (68)	92−95 (22)		38290	261	0.866	x	89−95 (73)	92−95 (19)	
OpZn2													
14530	688	0.953	y	75−76 (93)			39000	256	0.987	y	71−77 (46)	74−77 (44)	
16250	616	0.801	x	75−77 (91)			39310	254	1.343	y	74−77 (44)	71−77 (40)	
33300	300	1.079	x	71−76 (49)	74−76 (38)		40650	246	0.105	x	67−76 (53)	69−77 (26)	
34500	290	1.70	x	74−76 (45)	71−76 (38)		40760	245	0.258	y	69−76 (88)		
37370	268	0.079	x	75−81 (78)									
OpZn6													
13150	760	1.07	y	111−112 (96)			37010	270	0.243	y	108−113 (32)	111−123 (32)	
13710	729	1.313	x	111−113 (95)			37690	265	0.196	x	106−112 (80)		
22160	451	0.053	y	111−115 (97)			38410	260	0.204	y	111−123 (50)	108−113 (31)	
33070	302	0.361	x	109−113 (63)			39070	256	1.306	x	106−113 (72)		
33920	294	0.249	y	111−121 (81)			40250	248	1.054	y	110−114 (24)	111−127 (20)	109−115 (17)
35730	280	3.204	x	108−112 (81)			41510	241	0.22	y	111−127 (64)		
OpZn8													
12660	790	1.027	y	129−130 (96)			34820	287	3.736	x	126−130 (67)		
13390	747	1.569	x	129−131 (95)			35550	281	0.334	y	129−141 (74)		
19560	511	0.072	y	129−133 (94)			37490	267	0.104	x	124−130 (75)	118−130 (15)	
26180	382	0.093	x	129−136 (96)			38690	258	2.312	y	126−131 (63)		
28160	351	0.064	y	127−130 (67)	128−132 (20)		39180	255	0.156	x	129−146 (52)	129−152 (20)	
29650	337	0.345	x	127−131 (70)			39730	252	0.390	y	129−147 (34)	124−131 (25)	129−144 (18)
30680	326	0.226	y	129−138 (72)			40410	247	0.105	x	128−134 (14)		
33250	301	0.199	y	128−132 (33)	127−133 (29)	127−130 (17)	41280	242	0.081	y	129−147 (23)	128−137 (20)	

[a] Excited states with less than 42000 cm⁻¹, *f* > 0.05, and configurations which contribute more than 15% are shown. [b] Polarization. [c] Orbital numbers 57, 93, 75, 111, and 129 are HOMOs of TAP, Pc, AdZn2 and OpZn2, AdZn6 and OpZn6, and AdZn8, OpZn8, and Nc, respectively. In AdZn6 and OpZn6, the MOs numbered 109, 110, 114, and 115 are naphthalene-centered orbitals. In AdZn8 and OpZn8, the MOs numbered 127,128, 132, and 133 are anthracene-centered orbitals. In Nc, the MOs numbered 125, 126, 127, 128, 133, 134, and 135 are naphthalene-centered orbitals.
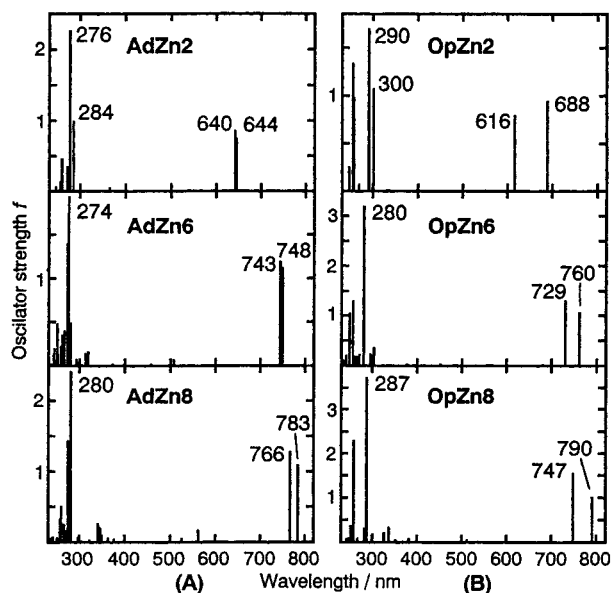
Figure 9. Calculated absorption spectra for the low symmetrical zinc derivatives in this study. (A) Adjacent species and (B) opposite species.

Corresponding to the experimental data obtained for adjacent molecules (Figure 3), the following information has been obtained from the calculations. (i) The Q-band shifts to longer wavelength, but the extent of this per two benzene units becomes smaller the larger the size of the molecules. The experimental energy differences were, after elimination of the substituent effect, ca. 1320 cm^{-1} for Co0−AdCo2, 1020 cm^{-1} for AdCo2−AdCo4, 837 cm^{-1} for AdCo4−AdCo6, and 520−740 cm^{-1} for AdCo6−AdCo8. The calculated corresponding values were 761, 1334, 824, and 503 cm^{-1}, respectively. (ii) Setting the relative intensity of the Q-band of Co0 at unity, the experimental ratios of the oscillator strengths for Co0:AdCo2:AdCo4:AdCo6:AdCo8 were 1.00:1.15:1.72:2.09:2.14. Calculations of the corresponding values gave 1.00:1.23:1.63:1.77:1.82 (comparison of *f* values in Table 4), indicating that the effect of fused benzene decreases the farther the benzene from the center of the molecule. (iii) The predicted splitting (293 cm^{-1}) of the Q-band of AdZn8 is, as seen in Figure 9A, much larger than that (98 cm^{-1}) of AdZn6. After obtaining this calculated result, we checked the experimental values for AdCo8 and AdCo6, and these were 353 and 237 cm^{-1}, respectively, assuming that the energy difference between the MCD trough and peak roughly represents the splitting (267 cm^{-1} for tetra-*tert*-butyl CoPc[17b]). (iv) Although the calculations estimate the Soret transition to lie at higher energy than experimentally observed, by ca. 4700−7900 cm^{-1}, the band position is rather insensitive to the size of the molecules, as is indeed observed (Figure 3A). (v) *x*- and *y*-axes polarized transitions are predicted on the longer wavelength side of the Soret band of AdZn6 at 318 and 312 nm (or 31 450 and 32 050 cm^{-1}) and of AdZn8 at ca. 363−376 and 341−349 nm (or 27 100 ± 500 and 29 000 ± 400 cm^{-1}). These are transitions involving mostly naphthalene- or anthracene-centered orbitals. These transitions may correspond to bands at 412 nm for AdCo6 and at 495 nm for AdCo8, since the MCD signal associated with these bands changes from plus to minus, viewing from the longer wavelength side (note that *x*- and *y*-axes polarized transitions in Table 4 give MCD signals of plus and minus, respectively, experimentally).

With respect to opposite type species, the following results have been obtained and are therefore compared with experiments. (vi) The Q-band splits into two, and the extent of the splitting is larger the larger the difference between the short and long axes of the molecule, as has been observed experimentally (Table 2). However, no obvious splitting was detected in the absorption spectra of OpCo2 (Figure 4A), despite this being substantiated to be the opposite type isomer by X-ray analysis (section (i)) (we will comments on this point later, below). (vii) If we define the center of the split Q-band as the positions of the Q-band, this is similar to the corresponding adjacent species, as expected from the symmetry-adapted perturbation theory.[4,5,29b] For OpZn2, OpZn6, and OpZn8, the positions are 650, 745, and 768 nm (or 15 380, 13 460, and 13 020 cm^{-1}), and the values for AdZn2, AdZn6, and AdZn8 were 642, 745, and 775 nm (or 15 580, 13 420, and 12 900 cm^{-1}). (viii) Calculated oscillator strengths of the Q-band of opposite species appear slightly (3−9%) larger than those of the corresponding adjacent species (Table 4), although it is difficult to detect this difference experimentally. (ix) The Soret band position does not depend markedly on the molecular size. In the case of OpZn6 and OpZn8, naphthalene- or anthracene-centered, short-axis polarized transitions have been predicted to the red of the Soret band.

(b) Molecular Orbital Energy Level. Figure 10 shows the calculated energies of some frontier orbitals. The main results may be summarized as follows. (i) The HOMO destabilizes, but to a decreasing extent with increasing molecular size, while the second HOMO of the macrocycle remains almost constant (note that there are several naphthalene- or anthracene-centered orbitals in the larger molecules, which are marked in the figure). (ii) The HOMO energy is similar between the corresponding opposite and adjacent isomers. (iii) The LUMO of opposite isomers split into two, and the differences are 5150, 1640, and 2270 cm^{-1} for OpZn2, OpZn6, and OpZn8, respectively. Since the Q-band is approximated as an almost pure one-electron transition (Table 2), these differences have a parallel relationship with the calculated splittings of the Q-band of these molecules (1717, 561, and 728 cm^{-1}, respectively). (iv) The splitting of the LUMO of adjacent species is small, if it occurs at all. (v) In agreement with the experimental fact that the Q-band of adjacently dinaphthalene-fused Pc's lies at shorter wavelength than that of naphthalocyanine (Nc),[17b] the calculated energy difference between the HOMO and LUMO in the former (28 500 cm^{-1}) is slightly larger than that of the latter (28 000 cm^{-1}), supporting the view that the effect of fusion of the outer benzene is smaller (note that the π system of these two species is isomeric).

(c) Interpretation of the Peculiarity of the Spectrum of OpCo2 from MO Calculations. Now we have to consider the apparent discrepancy between the experimental unsplit (Figure 4A) and predicted (by MO calculations), largely split Q-band spectra (Table 4) of oppositely dibenzo-substituted TAPs. As shown in our previous papers,[3c,q] we consider that the spectral shift of TAP derivatives can be explained by the SAP method.[4,5,29b] Lending support to this, the splitting of the Q-band estimated by the SAP method (1495 cm^{-1})[38−43] is not far away from the calculated value (1717 cm^{-1}) for OpZn2. Accordingly, we have to consider much higher order perturbations in explaining the Q-band of OpCo2. To obtain insight into this
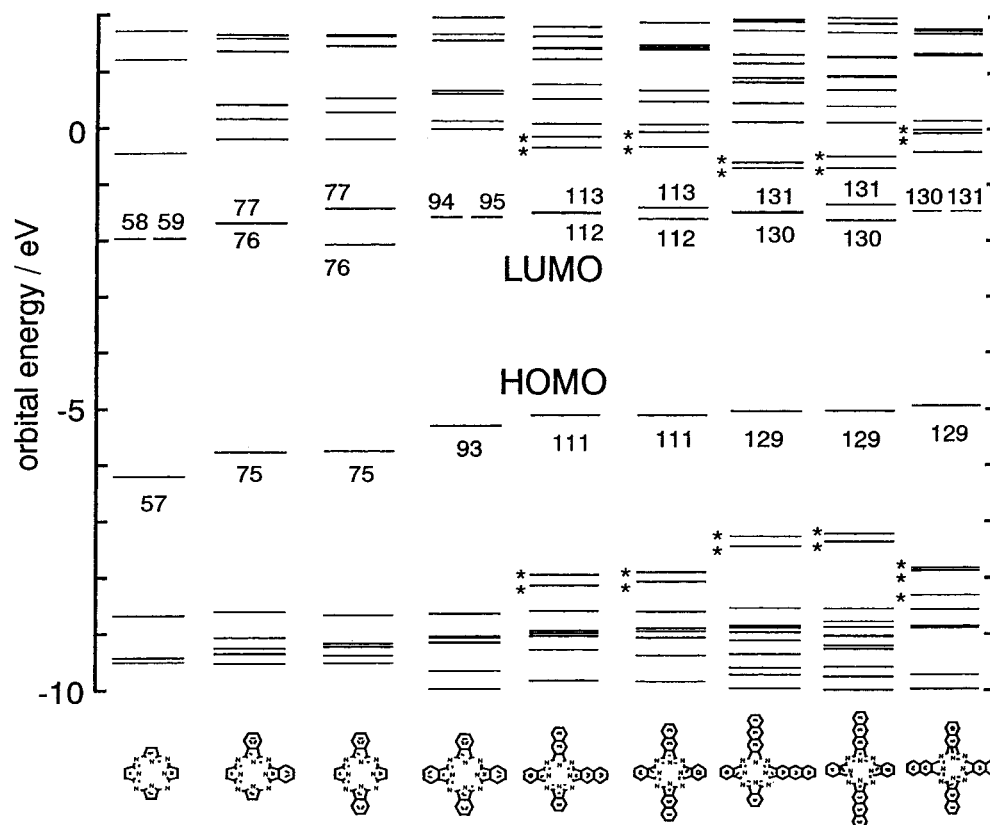
Figure 10. Partial molecular orbital energy diagram for skeletons containing zinc. Orbitals marked by ∗ indicate naphthalene- or anthracene-centered orbitals. Numbers indicate orbital number.

problem, we decided to calculate the MOs including substituent groups, although only π systems were taken into consideration in the above calculations.

The summary of calculations is shown stepwise in Figure 11. The introduction of four alkyl (methyl) groups at the 7,8,-

(38) Since the SAP method predicts how much the Q_{x00}- and Q_{y00}-bands shift from the doubly degenerate Q_{00}-band position, we have estimated the shift experimentally as follows. In OpCo2, four alkyl groups are linked to the TAP skeleton at the opposite positions along the *x*-axis, while two diphenylbenzo groups are fused at opposite positions along the *y*-axis. Unsubstituted MgTAP shows the Q_{00}-band at 586 nm (17 065 cm^{-1}) in CHCl$_3$,[38] while octaethylated MgTAP has the Q_{00}-band at 597 nm (16 750 cm^{-1}) in CH$_2$Cl$_2$.[39] Taking into account that the Q-band positions of TAPs and Pc's are almost the same in these two solvents and that an approximate additivity exists on the substituent effect,[24,25] the shift by four alkyl groups at opposite positions of the TAP skeletons is estimated to be ca. 158 $\{=(17\ 065 - 16\ 750)/2\}$ cm^{-1}, which corresponds to ca. 5–6 nm at around 600 nm. The substituent effect of the two *p*-diphenylbenzo groups can be estimated by comparing the data of metal-free species. If the center of the split Q-band is defined as the position of the Q-band, then that of OpH$_2$2 is at 646 nm in *o*-DCB. If we subtract the above contribution by four alkyl groups, it is inferred that the Q-band of two *p*-diphenylbenzo-substituted TAP lies at ca. 640 nm (15 625 cm^{-1}). On the other hand, since the center of the split Q-band of unsubstituted H$_2$TAP is at 579 nm (17 278 cm^{-1}) in chlorobenzene,[40] which is a similar solvent to *o*-DCB, the effect is calculated as ca. 1653 cm^{-1}. Although there is no absorption data on unsubstituted CoTAP,[41] tetra(cyclohexano) CoTAP, an octaalkylated CoTAP, shows a Q-band at 591 nm (16 920 cm^{-1}) in chlorobenzene.[42] Since the substituent effect of an octaalkyl group is 315 cm^{-1} from the above data on MgTAP, and the Q-band positions of Pc's and TAPs in chlorobenzene and toluene are very close,[24,41] the Q-band position of unsubstituted CoTAP in these solvents is estimated to lie at 580 nm (17 235 cm^{-1}). In this way, the two Q_{00}-band positions of OpCo2 calculated by the SAP method appear to lie at ca. 586 (17 235 − 158 = 17 077 cm^{-1}) and 642 nm (17 235 − 1653 = 15 582 cm^{-1}). The splitting estimated by the SAP method is, therefore, 1495 cm^{-1}.
(39) Stuzhin, P. A.; Khelevina, O. G. *Coord. Chem. Rev.* **1996**, *147*, 41.
(40) Ough, E. A.; Creber, K. A. M.; Stillman, M. J. *Inorg. Chim. Acta* **1996**, *246*, 361.
(41) Linstead, R. P.; Walley, M. *J. Chem. Soc.* **1952**, 4839.
(42) Kobayashi, N. In *The Porphyrin Handbook*; Kadish, K. M., Smith, K. M., Guilard, R., Eds.; Academic Press: New York, 1999; Vol. 2, Chapter 13.
(43) Ficken, C. E.; Linstead, R. P. *J. Chem. Soc.* **1952**, 4846.

Calculated				
Qx	688	691	699	699
Qy / nm	616	633	631	658
ΔQ / cm^{-1}	1717	1328	1538	908

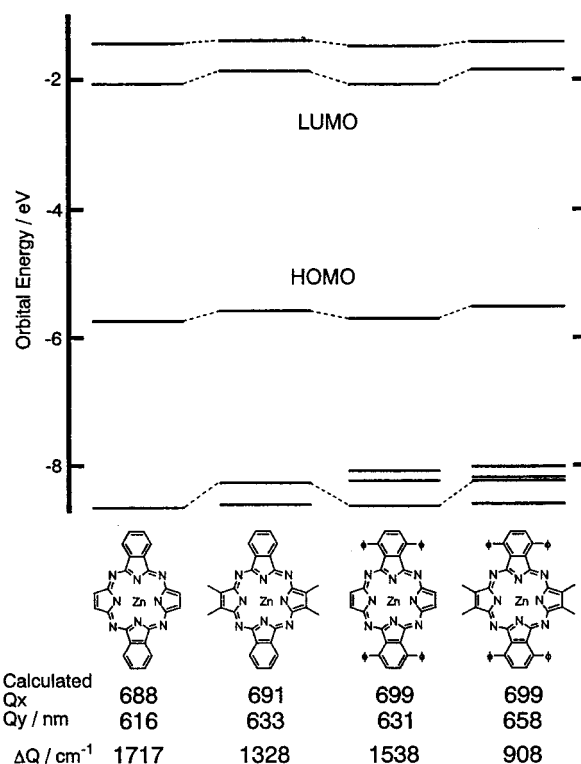**Figure 11.** Calculated frontier orbital energy of the OpZn2 π skeleton, OpZn2 substituted by four methyl groups at 7,8,17,18-positions, OpZn2 substituted by four phenyl groups at $2^1,2^4,12^1,12^4$-positions, and OpZn2 substituted by four methyl groups at 7,8,17,18-positions and four phenyl groups at $2^1,2^4,12^1,12^4$-positions. Numbers below each structure indicate the predicted Q-band position and splitting energy.
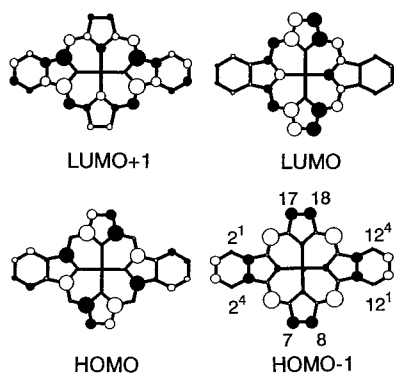
Figure 12. Four frontier orbitals of OpZn2. The positions 7, 8, 17, and 18, to which alkyl groups are linked, and the positions 2^1, 2^4, 12^1, and 12^4, to which phenyl groups are connected, are indicated in one of the figures.

17,18-positions and of four phenyl groups at the $2^1,2,^412^1,12^4$-positions decreased the Q-band splitting compared to the parent molecule (1717 cm^{-1}) to 1328 and 1538 cm^{-1}, respectively, and when both the alkyl and phenyl groups were included in the calculations, the value became nearly half (908 cm^{-1}).[44] These data suggest that the substituents do lessen the splitting of the Q-band and that the effect of four alkyl groups is larger than that of four phenyl groups, although generally the substituent effect of the latter group is more significant.[2,24] This inverse trend can be reasonably explained by considering the size of the coefficient of carbons in frontier MOs in Figure 12. As can be seen, the coefficients of carbons at the 7,8,17,18-positions are much larger than those at $2^1,2,^412^1,12^4$-positions of the opposite dibenzoTAP skeleton, where four phenyl groups are bound except in the case of the LUMO+1, indicating that the substituent effect can appear much more sensitively at the former four positions. This is indeed reflected in the change of MO energy (Figure 11, top). When four phenyl groups were introduced at $2^1,2,^412^1,12^4$-positions of the opposite dibenzoTAP skeleton, the energy of the four frontier orbitals changed slightly, while linking four alkyl groups to the 7,8,17,18-positions substantially destabilized the HOMO−1, HOMO, and LUMO, and as a result, the LUMO and LUMO+1 levels approach each other. Then, since more than 90% of the Q-band is composed of the HOMO-to-LUMO and LUMO+1 transitions (Table 5), the splitting of the Q-band also becomes smaller.

(d) Interpretation of the Split MLCT Band of AdCo^{I}2 and OpCo^{I}2 Species. The main results of the MO calculations on Co(I) species are summarized in Table 6. The MLCT bands observed experimentally at 470 and ca. 425−430 nm for Co^{I}Pc were reproduced at 415 and 381 nm (or 24 100 and 26 350 cm^{-1}).[33,36] These are transitions from the HOMO−1 (e$_g$ dπ) to

(44) To confirm even a part of these substituent effects experimentally, we have prepared two compounds, i.e., [$2^1,2^4,12^1,12^4$-tetraphenyldibenzo[*b,l*]-5,10,-15,20-tetraazaporphyrinato(2−)]zinc(II) $C_{48}H_{28}N_8Zn$ {Mass (ESI-TOF) (*m/z*): 781 ([M + 1]$^+$). ^{1}H NMR (400 MHz, CDCl$_3$ + 2% C$_5$D$_5$N): δ 7.76 (m, 12H, phenyl *m*-, *p*-H), 8.08 (s, 4H, arom H), 8.28 (d, 8H, phenyl *o*-H), 8.73 (s, 4H, arom H). UV−vis (CHCl$_3$) λ_{max}: 339, 572, 625, 667.} and [$2^1,2^4,12^1,12^4$-tetraphenyldibenzo[*b,l*]-7,8,17,18-tetrapropyl-5,10,15,20-tetraazaporphyrinato(2−)]zinc(II) $C_{60}H_{52}N_8Zn$ {Mass (ESI-TOF) (*m/z*): 949 ([M + 1]$^+$). UV−vis (CHCl$_3$) λ_{max}: 341, 587, 645.}. The former compound exhibited Q-band peaks at 625 and 667 nm (splitting energy = 1007 cm^{-1}), while the latter showed a single relatively broad Q-band peak at 645 nm with a half-width of 779 cm^{-1} (the half-width of the Q-band at 593 nm of tetra-*tert*-butylated ZnTAP in the same solvent is ca. 570 cm^{-1} (our unpublished data)), which may be produced by a superimposition of closely lying Q$_{y00}$ and Q$_{x00}$ bands. The splitting of the Q-band of the latter compound appears at 360 cm^{-1}, estimated from the energy difference between the MCD trough (655 nm) and peak (640 nm) of the Q-band. Thus, four alkyl groups indeed function to reduce the Q-band splitting.

Table 5. Calculated Transition Energies, Oscillator Strength (*f*), and Configurations^a

energy/ cm^{-1}	nm	*f*	pol.^{b}	configurations^c	
			OpZn2Me4		
14470	691	0.888	*y*	87−88 (93)	86−89 (6)
15800	633	0.757	*x*	87−89 (91)	86−88 (7)
			OpZn2Ph4		
14310	699	0.955	*y*	131−132(93)	128−133 (6)
15850	631	0.893	*x*	131−133(93)	128−132 (6)
			OpZn2Me4Ph4		
14300	699	0.890	*y*	143−144(93)	140−145 (6)
15200	658	0.864	*x*	143−145(93)	140−144 (6)

^{a} Only Q-bands are shown. ^{b} Polarization. ^{c} Orbital numbers 87, 131, and 143 are HOMOs of OpZn2Me4, OpZn2Ph4, and OpZn2Me4Ph4, respectively.

the LUMO+1 (b$_{1u}$*) and LUMO+2 (b$_{2u}$*). Similarly, the corresponding band observed at 519 nm for Co^{I}TAP was reproduced at 457 nm (21 900 cm^{-1}).[17a] For OpCo^{I}2, the split MLCT bands were calculated at 426 (23 470 cm^{-1}, *f* = 0.571, polarization = *y*) and 383 nm (26 110 cm^{-1}, *f* = 0.941, polarization = *x*). These were almost pure one-electron transitions from the HOMO−1 (b$_{1g}$ dπ) to LUMO+2 (a$_u$ π*) and LUMO+3 (b$_{3u}$ π*) orbitals, respectively, in D_{2h} symmetry. From the relative intensity ratio and the difference between the observed and calculated wavelengths, these transitions appear to correspond to two peaks at ca. 559 and 493 nm of OpCo^{I}2 in Figure 7B. In the case of AdCo^{I}2, MLCT transitions (mostly from the HOMO−1 (b$_1$ dπ) and HOMO−2 (a$_2$ dπ) to the LUMO+1∼4 π*) are calculated at 433 (23 100, 0.078), 400 (25 000, 0.273), 397 (25 200, 0.112), 373 (26 810, 0.170), 370 (27 030, 0.084), 346 (28 900, 0.368), and 343 (29 150, 0.183) nm, since many transitions are allowed and can mix with π−π* transitions in C_{2v} symmetry. From the configuration, the contributions of π−π* transitions to the bands estimated at 400, 397, 373, 346, and 343 nm are ca. 42, 44, 28, 46, and 25%, respectively. The above results suggest the presence of three peaks at ca. 430 (weak), 390−400 (medium), and 340−350 (strong) nm. These bands may correspond to an experimental weak peak at ca. 550 nm, a medium peak at 525 nm, and an intense peak at 458 nm for AdCo^{I}2 in Figure 7A.

Conclusions

We have succeeded in preparing a series of adjacent and opposite type di-aromatic ring-fused cobalt Pc derivatives of varying size. The spectroscopic properties have been examined using electronic absorption and magnetic circular dichroism spectroscopies, together with electrochemical methods, and most of the properties have been reproduced by MO calculations using the ZINDO/S Hamiltonian. The adjacent isomers have been obtained preferentially on their own by using a diphthalonitrile unit linked via a short aryl chain. The Q-band shifts to longer wavelength, and its intensity increases but the extent decreases with increasing molecular size. The substituent effect caused by fusion of benzene on the Q-band position decreases with increasing separation of the benzene unit from the center of the tetraazaporphyrin skeleton. Setting the magnitude of the effect of benzene directly fused to the TAP skeleton at unity, the effect of the second and third benzene units is roughly about 0.75− 0.80 and 0.48 ± 0.06, respectively. On ring annulation, the HOMO destabilizes significantly, while the LUMO remains

Table 6. Calculated Transition Energies, Oscillator Strength (*f*), and Configurations of Cobalt(I) Species

λ/nm	ν/cm⁻¹	*f*	obsd[a]	pol.[b]	configurations[c]			assignment
					CoTAP			
569	17590	0.458	624 (16030)		61→63 (87)			Q
569	17590	0.458			61→62 (87)			Q
457	21870	0.213	519 (19270)	*y*	60→64 (95)			MLCT
457	21870	0.213		*x*	59→64 (95)			MLCT
323	31010	0.074		*x*	60→65 (77)	56→63 (18)		MLCT
323	31010	0.074		*y*	59→65 (77)	56→62 (18)		MLCT
					OpCo2			
615	16270	0.468	672 (14880)	*y*	79→81 (94)			Q
542	18440	0.557		*x*	79→80 (91)			Q
426	23490	0.571	559 (17890)	*y*	78→82 (93)			MLCT
383	26120	0.941	493 (20280)	*x*	78→83 (83)			MLCT
317	31580	0.105		*x*	77→82 (80)			MLCT
					AdCo2			
599	16710	0.588	664 (15060)	*x*	79→80 (84)	77→80 (7)		Q
596	16770	0.567		*y*	79→81 (90)			Q
433	23110	0.078	525 (19050)	*x*	77→82 (65)	79→82 (26)		MLCT, π−π*
400	25010	0.273	458 (21830)	*y*	79→83 (42)	77→83 (24)	78→82 (19)	MLCT, π−π*
397	25200	0.112		*x*	79→82 (44)	78→83 (33)		MLCT, π−π*
373	26790	0.170		*x*	79→82 (28)	78→83 (25)	77→82 (24)	MLCT, π−π*
370	27030	0.084		*y*	78→80 (24)	78→84 (24)	77→81 (21)	MLCT, π−π*
346	28930	0.368		*x*	79→84 (46)	77→84 (23)	78→83 (18)	MLCT, π−π*
343	29170	0.183		*y*	77→83 (38)	79→83 (25)	77→87 (12)	MLCT, π−π*
					CoPc			
649	15410	0.723	708 (14120)		97→98 (47)	97→99 (46)		Q
649	15410	0.723			97→99 (47)	97→98 (46)		Q
415	24110	0.108	471 (21230)		96→101 (52)	95→100 (22)	97→104 (16)	MLCT
415	24110	0.108			95→101 (52)	96→100 (22)	97→103 (16)	MLCT
381	26250	0.562	435 (22990)		96→100 (70)	95→101 (21)		MLCT
381	26250	0.562			95→100 (70)	96→101 (21)		MLCT

[a] Observed band wavelength (nm) and energies (cm⁻¹) from the data reported in this paper (OpCo2 and AdCo2), in Kobayashi, N.; Nakajima, S.; Osa, T. *Chem. Lett.* **1992**, 2415 (CoTAP), and in Nevin, W. A.; Hempstead, M. R.; Liu, W.; Leznoff, C. C.; Lever, A. B. P. *Inorg. Chem.* **1987**, *26*, 570 (CoPc). [b] Polarization. On the direction of *x,y*, see Figure 1. [c] Values in parentheses indicate the contribution (%) of the configuration. Numbers at both sides of arrows indicate orbital numbers. CoTAP (HOMO: 61; LUMO: 62; dπ: 59, 60; dz2:58; dxy: 57), OpCo2 (79; 80; 77, 78; 76; 74), AdCo2 (79; 80; 77, 78; 76; 75), CoPc (97; 98; 95, 96; 94; 93), AdCo6 (115; 116; 113, 114; 112; 111), AdCo8 (133; 134; 131, 132; 130; 127), CoNc (133; 134; 131, 132; 130; 129).

almost constant. In the adjacently substituted series, a single Q-band is observed, while in the oppositely substituted species, split Q-bands are generally observed, except in the case of an oppositely dibenzo-fused dialkylated TAP. The extent of the splitting of the Q-band of oppositely substituted species has a parallel relationship with the splitting of the LUMO of these species, which in turn relates to the ratio of long to short axes in the molecule. Thus, the larger the ratio, the larger the splitting. The first oxidation in adjacently and oppositely dibenzo-fused CoTAP occurs at the cobalt and ligand, respectively. A small splitting of the Q-band of an oppositely dibenzo-fused alkylated TAP and split MLCT bands observed for two dibenzo-substituted Co^I TAP are reasonably explained in terms of MO calculations.

Supporting Information Available: Tables of crystal data and structure refinement, atomic coordinates and equivalent isotropic displacement parameters, bond lengths and angles, and aniso-tropic displacement parameters for OpCo2; calculated and observed isotropic distribution patterns of the mass spectra of all cobalt complexes; and band-fitting parameters for the spectra of Co0, AdCo2, AdCo4, AdCo6, and AdCo8 in toluene (PDF). This material is available free of charge via the Internet at http://pubs.acs.org. CCDC 180877 contains the supplementary crystal-lographic data for this paper. These data can be obtained free of charge via www.ccdc.cam.ac.uk/conts/retrieving.html (or from the Cambridge Crystallographic Data Centre, 12 Union Rd., Cambridge CB2 1EZ, UK; deposit@ccdc.cam.uk).

JA0123812